

---

# *DCoM*: Active Learning for All Learners

---

**Inbal Mishal<sup>†</sup>, Daphna Weinshall<sup>†</sup>**  
 School of Computer Science & Engineering<sup>†</sup>  
 The Hebrew University of Jerusalem  
 Jerusalem 91904, Israel  
 {inbal.mishal,daphna}@mail.huji.ac.il

## Abstract

Deep Active Learning (AL) techniques can be effective in reducing annotation costs for training deep models. However, their effectiveness in low- and high-budget scenarios seems to require different strategies, and achieving optimal results across varying budget scenarios remains a challenge. In this study, we introduce Dynamic Coverage & Margin mix (*DCoM*), a novel active learning approach designed to bridge this gap. Unlike existing strategies, *DCoM* dynamically adjusts its strategy, considering the competence of the current model. Through theoretical analysis and empirical evaluations on diverse datasets, including challenging computer vision tasks, we demonstrate *DCoM*'s ability to overcome the cold start problem and consistently improve results across different budgetary constraints. Thus *DCoM* achieves state-of-the-art performance in both low- and high-budget regimes.

## 1 Introduction

Deep Learning (DL) algorithms require a lot of data to achieve optimal results. In certain scenarios, there is an abundance of unlabeled data but limited capacity for labeling it. In fields such as medical imaging, an invaluable resource — doctors themselves — serves as a costly oracle. Active learning algorithms aim to address this challenge by reducing the burden of labeling and making it more effective. Unlike traditional supervised learning frameworks, Active Learning (AL) can affect the construction of the labeled set, possibly by leveraging knowledge about the current learner. Accordingly, the initial goal of AL is to select  $q$  examples to be annotated, where  $q$  represents the number of examples that can be sent to the oracle. AL has already demonstrated tangible contributions across various domains such as computer vision tasks [40], NLP [31, 20] and medical imaging [10]. These examples highlight the importance of advancing AL to achieve even greater impact.

The choice of an AL strategy depends on both the learner's inductive biases and the nature of the problem. Recent research suggests that the optimal active learning strategy varies with the budget size, where budget refers to the size of the training set. When the budget is large, methods based on uncertainty and diversity sampling are most effective. Conversely, when the budget is small, methods centered on typicality and diversity are more appropriate. However, there is no single active learning strategy that is suitable for all budget regimes. Our study aims to address this challenge by dynamic selection of the best examples based on the current state of the learner and the current budget.

As briefly reviewed below, recent research often categorizes active sampling methods according to the budget regime. In contrast, our study takes a different approach by recognizing the need to adapt sample selection methods based on the learner's competence. We aim to develop a single algorithm that dynamically adjusts its sampling strategy in response to the learner's evolving abilities. This transition from budget to learner's competence represents a significant advancement in active learning research, as it allows us to move beyond rigid budget allocations and towards a more adaptive approach that optimizes performance based on the learner's abilities.

In this work, we introduce a novel method called Dynamic Coverage & Margin mix (*DCoM*), which dynamically adjusts its selection strategy to deliver optimal results. We begin by examining a

simplified theoretical framework (Section 2), where we integrate a typicality test with an uncertainty test based on the budget and its coverage. Inspired by the insights gained from this analysis, we introduce *DCoM* (Section 3), which combines these characteristics. *DCoM* aims to offer a flexible solution for any budget by selecting the most appropriate examples that are most suitable to the current budget. We validate *DCoM* through an extensive empirical study using various vision datasets (Section 4). Our findings indicate that *DCoM* effectively achieves superior performance across all budget ranges.

**Relation to prior art.** Over the past years, active learning has been an active area of research [34, 29, 7, 32]. The realm of Active Learning (AL) is segmented into three problem settings: membership query synthesis, stream-based selective sampling, and pool-based active learning [29]. The majority of current AL research adheres to the pool-based AL setting, where samples are drawn from a vast pool of unlabeled data and annotations are solicited from an oracle. In this setting, AL algorithms operate within a given budget ( $b$ ), selecting a subset of unlabeled examples to send to an oracle for labeling. This selection process aims to identify examples that will maximize the model’s performance. This process may be repeated iteratively, gradually increasing budget  $b$ .

In discussions of pool-based AL, two key characteristics that play a crucial role during the active sampling process are *uncertainty* and *diversity*. Some AL algorithms focus solely on uncertainty sampling [23, 30, 4, 43, 18, 12, 27, 37, 11], while others prioritize diversity sampling [28, 19, 39, 15]. Other algorithms combine both uncertainty and diversity in their approaches [38, 2, 36, 21, 5, 1].

Over time, the cold start problem emerged, highlighting the challenges faced by AL algorithms when operating with a small budget. It seems that *uncertainty* and *diversity* do not capture this difficulty. Chen et al. [2], for example, describe the cold start problem as a combination of two issues: unbalanced sampling across different classes (which relates to diversity) and unbalanced sampling within each class, where uncertain examples are favored over certain ones at the outset.

In low-budget scenarios, typical examples often offer the best outcomes for the model [2, 39, 15, 14]. This implies that in such contexts, AL algorithms should aim to maximize both certainty and diversity. Conversely, in high-budget scenarios, the emphasis shifts towards maximizing uncertainty while maintaining diversity. [14] proposes a method to select the most suitable approach based on the current state. This method involves comparing multiple active learning strategies during runtime, rather than recommending a single universal approach.

**Summary of contribution.** (i) Expand a theoretical framework to analyze Active Learning (AL) strategies in embedding spaces. (ii) Introduce *DCoM*, a multi-budget strategy that significantly outperforms previous methods in low and medium budget scenarios and matches their performance in high budget scenarios. (iii) Initiates a transition from a budget-based approach to the learner’s competence, introducing coverage as a measure designed to predict this competence.

## 2 Theoretical framework

The framework of active learning adopted here can be formalized as follows: Let  $\mathbb{X}$  denote the input domain,  $\mathbb{Y}$  the target domain, and  $\mathcal{L} : \mathbb{X} \rightarrow \mathbb{Y}$  the target learner. Before seeing any labels,  $\mathcal{L}$  may be a random feasible hypothesis, or it may be initialized by either transfer learning or self training.

Active learning may involve a single step, or an iterative process with repeated active learning steps. In each step of active learning, the learner actively seeks labels by choosing a set of unlabeled points as a query set, to be labeled by an oracle/teacher. Subsequently, this set of labeled points is added to the learner’s supervised training set, and the learner is retrained or fine-tuned.

As discussed in the introduction, it has been shown that different active learning strategies are suitable for different budgets  $b$ . Henceforth,  $b$  refers to the number of labeled examples known to the learner at the beginning of an active learning step. With a low budget  $b$ , strategies that do not rely on the outcome of the learner are most suitable. When  $b$  is high, it is beneficial to take into consideration the confidence of the learner when choosing an effective query set. What makes a budget high or low was left vague in previous analysis, as it clearly depends on the specific application and dataset.

To achieve an effective active learning protocol suitable for all learners, irrespective of budget, we aim to devise a universal objective function, whose minimization is used to select the query set. Next, we discuss its envisioned form for selecting the query set at the beginning of each AL step.

We begin our discussion by proposing to replace the notion of *budget* with the notion of *competence*: a network is competent if its generalization score is relatively high, and vice versa. This proposal is more formally justified in Section 2.3. We then rephrase the intuition stated above as follows: When the learner’s competence is low, the objective function should prioritize typicality and diversity of selected queries (see discussion in the introduction) irrespective of the learner’s predictions. When the learner’s competence is high, its uncertainty in prediction should be given high priority.

More formally, let  $\mathcal{O}(x)$  denote the desired objective function for query selection, where  $x \in \mathbb{X}$  is unlabeled. Let  $\mathcal{O}_{low}(x)$  and  $\mathcal{O}_{high}(x)$  denote the objective functions suitable for a learner with low competence and high competence respectively. Let  $S_{\mathcal{L}}$  denote a score, which captures the competence of learner  $\mathcal{L}$ . The proposed objective function can now be written as follows  $\forall x \in \mathbb{X}$ :

$$\mathcal{O}(x) = (1 - S_{\mathcal{L}}) \cdot \mathcal{O}_{low}(x) + S_{\mathcal{L}} \cdot \mathcal{O}_{high}(x) \quad (1)$$

In Section 2.2 we discuss the design of  $\mathcal{O}_{low}(x)$ . In order to tackle the challenge of active learning when the competence of  $\mathcal{L}$  is low, we utilize the point coverage framework introduced in [39]. This approach relies on self-supervised data representation, which is blind to the learner’s performance. We refine their analysis and obtain an improved generalization bound for the 1-Nearest Neighbor (1-NN) classification model that depends on the local geometry of the data. Beforehand, in Section 2.1 we discuss the necessary preliminaries required to introduce the coverage approach. In Section 2.3 we discuss our choice of  $S_{\mathcal{L}}$ , and connect it to the notion of budget discussed in previous work.

We select  $\mathcal{O}_{high}(x)$  to equal one minus the normalized lowest response between the two highest softmax outputs of  $\mathcal{L}$  at  $x$ , or *Margin*, as this is a common measure of prediction uncertainty.

## 2.1 Preliminaries

**Notations.** Let  $P$  denote the underlying probability distribution of data  $\mathbb{X}$ . Assume that a true labeling function  $f : \mathbb{X} \rightarrow \mathbb{Y}$  exists. Let  $\mathbb{U} \subseteq \mathbb{X}$  denote the unlabeled set of points, and  $\mathbb{L} \subseteq \mathbb{X}$  the labeled set, such that  $\mathbb{X} = \mathbb{U} \cup \mathbb{L}$ . Here  $|\mathbb{L}| = b \leq m$  is the annotation budget where  $|\mathbb{X}| = m$ .

Let  $B_{\delta}(x) = \{x' \in \mathbb{X} : \|x' - x\|_2 \leq \delta\}$  denote a ball of radius  $\delta$  centered at  $x$ . Let  $C \equiv C(\mathbb{L}, \delta) = \bigcup_{x \in \mathbb{L}} B_{\delta}(x)$  denote the region covered by  $\delta$ -balls centered at the labeled examples in  $\mathbb{L}$ . We call  $C(\mathbb{L}, \delta)$  the *covered region*, where  $P(C)$  denotes its probability. Let  $f^N$  denote the 1-NN classifier, and  $\mathcal{L}$  denote our current learner – a 1-NN classifier based on  $\mathbb{L}$ .

**Definition 2.1.** We say that a ball  $B_{\delta}(x)$  is *pure* if  $\forall x' \in B_{\delta}(x) : f(x') = f(x)$ .

**Definition 2.2.** We define the *purity* of  $\delta$  as

$$\pi(\delta) = P(\{x \in \mathbb{X} : B_{\delta}(x) \text{ is pure}\}).$$

Notice that  $\pi(\delta)$  is monotonically decreasing, as can be readily verified.

In [39] it is shown that the generalization error of the 1-NN classifier  $f^N$  is bounded as follows

$$\mathbb{E}[f^N(x) \neq f(x)] \leq (1 - P(C(\mathbb{L}, \delta))) + (1 - \pi(\delta)). \quad (2)$$

Subsequently, an algorithm is proposed that minimizes the first term in (2) by maximizing the coverage probability  $P(C(\mathbb{L}, \delta))$ , while ignoring the second term that is assumed to be fixed.

Below, we begin by refining the bound, focusing more closely on its second term  $(1 - \pi(\delta))$ . This is used in Section 3 to devise an improved algorithm that minimizes simultaneously both terms of the refined error bound.

## 2.2 Refined error bound

Define the indicator random variable  $I_{\delta}(x) = \mathbb{1}_{\{x \in \mathbb{X} : B_{\delta}(x) \text{ is pure}\}}$ . By definition,

$$\pi(\delta) = P(\{x \in \mathbb{X} : B_{\delta}(x) \text{ is pure}\}) = \mathbb{E}[I_{\delta}(x)].$$

Since the distribution of  $\mathbb{X}$  is not known apriori, we use the *empirical distribution* to approximate the expected value of this random variable. In accordance, given a labeled set  $\mathbb{L} = \{x_i\}_{i=1}^b$ :

$$\begin{aligned} \hat{\pi}(\delta) &= \hat{\mathbb{E}}[\mathbb{1}_{\{x \in \mathbb{L} : B_{\delta}(x) \text{ is pure}\}}] = \frac{1}{b} \mathbb{E}\left[\sum_{i=1}^b \mathbb{1}_{\{B_{\delta}(x_i) \text{ is pure}\}}\right] = \frac{1}{b} \sum_{i=1}^b \mathbb{E}[\mathbb{1}_{\{B_{\delta}(x_i) \text{ is pure}\}}] \\ &= \frac{1}{b} \sum_{i=1}^b P(B_{\delta}(x_i) \text{ is pure}). \end{aligned} \quad (3)$$

With this approximation

$$\mathbb{E} [f^N(x) \neq f(x)] \leq \left[1 - P(C(\mathbb{L}, \delta))\right] + \left[1 - \frac{1}{b} \sum_{i=1}^b P(B_{\delta_i}(x_i) \text{ is pure})\right] + \varepsilon. \quad (4)$$

where  $\varepsilon$  bounds the error of the empirical approximation in (3).

Note that the refined bound in (4) depends on the purity separately at each labeled point in  $\mathbb{L}$ . We further refine this bound by allowing the fixed radius  $\delta$  to be chosen individually, where  $\delta_i$  denotes the radius of point  $x_i \in \mathbb{L}$ . Let  $\Delta = [\delta_i]_{i=1}^b$  denote the list of individual radii corresponding to  $\mathbb{L} = \{x_i\}_{i=1}^b$ . The cover defined by  $\Delta$  is  $C(\mathbb{L}, \Delta) = \bigcup_{(x_i, \delta_i) \in \mathbb{L} \times \Delta} B_{\delta_i}(x_i)$ .

We consider the *normalized Nearest Neighbor* (nNN) classification algorithm, where the nearest neighbor is chosen by solving  $f^N(x) = \operatorname{argmin}_{x_i \in \mathbb{L}} \frac{d(x, x_i)}{\delta_i}$ . The bound on the error in (4) becomes

$$\mathbb{E} [f^N(x) \neq f(x)] \leq \left[1 - P(C(\mathbb{L}, \Delta))\right] + \left[1 - \frac{1}{b} \sum_{i=1}^b P(B_{\delta_i}(x_i) \text{ is pure})\right] + \varepsilon. \quad (5)$$

### 2.3 Competence score $S_{\mathcal{L}}$

In order to obtain a useful competence score<sup>1</sup>, which can be effectively used in objective function (1), we require that it satisfies the following conditions:

- (i) Lie in the range  $[0, 1]$ .
- (ii) Use all the data.
- (iii) Monotonically increase with the competence of learner  $\mathcal{L}$ .

In accordance, we propose to use the probability of coverage:

$$S_{\mathcal{L}}(\mathbb{L}, \Delta) = \frac{1 + e^{-k(1-a)}}{1 + e^{-k(P(C(\mathbb{L}, \Delta)) - a)}} \quad (6)$$

This function follows a logistic growth curve, with parameters defined as follows:  $a \in (0, 1)$  is the midpoint and  $k \in (0, \infty)$  determines the curve's steepness.

First, we note that this score satisfies the conditions stated above for the nNN classifier: (i)-(ii), as it is a function in  $[0, 1]$  that depends on all the data  $\mathbb{X}$ , while (iii) follows from the error bound (5). Below, we prove that it is also monotonically increasing with budget  $b$ .

More specifically, prior work showed empirically and theoretically that the training budget  $b = |\mathbb{L}|$  provides a useful clue for the desirable trade-off between  $\mathcal{O}_{low}(x)$  and  $\mathcal{O}_{high}(x)$  in (1), which is captured by score  $S_{\mathcal{L}}(\mathbb{L}, \Delta)$  defined in (6). We next show that  $S_{\mathcal{L}}(\mathbb{L}, \Delta)$  is monotonically increasing with  $b$ . This implies that definition (6) agrees with empirical evidence in prior work.

**Proposition.** For two labeled sets  $\mathbb{L}, \mathbb{L}'$ , if  $\mathbb{L} \subseteq \mathbb{L}'$  then  $S_{\mathcal{L}}(\mathbb{L}, \Delta) \leq S_{\mathcal{L}}(\mathbb{L}', \Delta')$ .

*Proof.* First, we note that

$$\mathbb{L} \subseteq \mathbb{L}' \implies C(\mathbb{L}, \Delta) = \bigcup_{x_i \in \mathbb{L}} B_{\delta_i}(x_i) \subseteq \left( \bigcup_{x_i \in \mathbb{L}} B_{\delta_i}(x_i) \right) \cup \left( \bigcup_{x_i \in \mathbb{L}' \setminus \mathbb{L}} B_{\delta_i}(x_i) \right) = C(\mathbb{L}', \Delta')$$

Since probability is monotonic, it follows that  $P(C(\mathbb{L}, \Delta)) \leq P(C(\mathbb{L}', \Delta'))$ . From (6), and by the definition of the logistic function using the provided parameters limits,  $S_{\mathcal{L}}(\mathbb{L}, \Delta)$  is monotonically increasing in  $\mathbb{L}$ , which implies that  $S_{\mathcal{L}}(\mathbb{L}, \Delta) \leq S_{\mathcal{L}}(\mathbb{L}', \Delta')$ .  $\square$

<sup>1</sup>When the labeled set  $\mathbb{L}$  is large, it may be possible to set aside a validation set to directly estimate the competence of learner  $\mathcal{L}$ , but this is not feasible when the labeled set  $\mathbb{L}$  is small.

### 3 Our method: *DCoM*

The error bound in (5) guides our method for active query selection, which aims to minimize this bound by maximizing the coverage  $P(C(\mathbb{L}, \Delta))$  and individual purity  $\pi(\delta_i) = P(B_{\delta_i}(x_i) \text{ is pure})$ . Recall that  $\mathbb{L}$  denotes the set of labeled points,  $\delta_i$  the influence radius of  $x_i \in \mathbb{L}$ ,  $\Delta = [\delta_i]_{i=1}^b$ , and

$$C(\mathbb{L}, \Delta) = \bigcup_{(x_i, \delta_i) \in \mathbb{L} \times \Delta} B_{\delta_i}(x_i), \quad \pi(\delta_i) = P(\{x \in B_{\delta_i}(x_i) : f(x) = f(x_i)\})$$

Since it was shown in [39] that maximizing  $P(C(\mathbb{L}, \delta))$  is already NP-hard, we opt for developing a greedy algorithm for actively selecting the query set, to be termed *DCoM*.

#### 3.1 Active learning method

The algorithm involves several steps:

- Initialization:** Define a suitable embedding space for the data and initialize essential parameters.
- If**  $\mathbb{L} \neq \emptyset$ , train model  $\mathbb{M}$  on  $\mathbb{L}$ , and compute  **$\delta$ -expansion** on the elements of  $\mathbb{L}$ . Otherwise,  $\Delta = [\delta_i = \delta_0]_{i=1}^b$ .
- Repeat** /\* iterative active learning steps \*/
  - (i) **Active query selection:** determine which examples to select for annotation.
  - (ii) **Model training:** obtain labels and train a deep learning model  $\mathbb{M}$ .
  - (iii)  **$\delta$ -expansion:** use  $\mathbb{M}$  to update  $\delta_i$  for the recently selected examples.
- Until** the accumulated budget is exhausted.

We next provide a detailed description of each step.

**Initialization:** We begin by seeking a suitable embedding space using  $\mathbb{U} \cup \mathbb{L}$ , where distances are intended to be inversely correlated with semantic similarity. Self-supervised or representation learning may be used to this end. We choose an initial radius  $\delta_0$  as described in [39].

(i) **Active query selection:** In this phase (see Alg 1 below for pseudo-code), the algorithm selects  $q$  examples from  $\mathbb{U}$  to send for labeling, where  $q$  denotes the query set size. To this end, it first computes several parameters:

---

#### Algorithm 1 *DCoM*, Active sampling

---

- 1: **Input:** unlabeled pool  $\mathbb{U}$ , labeled pool  $\mathbb{L}$ , query size  $q$ , list of ball sizes  $\Delta$ , trained model  $\mathbb{M}$  if  $\mathbb{L} \neq \emptyset$
  - 2: **Output:** a set of points to query, and the coverage of  $\mathbb{L}$
  - 3:  $\forall x \in \mathbb{U}, M(x) \leftarrow$  normalized margin between the two highest softmax outputs of  $\mathbb{M}$  if  $\mathbb{L} \neq \emptyset$ , 1 otherwise
  - 4: Compute  $P(C(\mathbb{L}, \Delta))$
  - 5: Compute  $S_{\mathcal{L}}(\mathbb{L}, \Delta)$
  - 6:  $\delta_{\text{avg}} \leftarrow \text{Average}(\Delta)$
  - 7:  $G = (V = \mathbb{U} \cup \mathbb{L}, E = \{(x, x') : x' \in B_{\delta_{\text{avg}}}(x)\})$
  - 8: **for**  $(x_i, \delta_i) \in \mathbb{L} \times \Delta$  **do**
  - 9:    $\forall x \in B_{\delta_i}(x_i) : \forall e = (v, x) \in E$ , remove  $e$  # DON'T COVER POINTS TWICE
  - 10:    $\forall e = (x_i, v) \in E$ , remove  $e$
  - 11: **end for**
  - 12:  $Q \leftarrow \emptyset$
  - 13: **for**  $i = 1, \dots, q$  **do**
  - 14:    $\forall x \in \mathbb{U}, \text{ODR}(x) \leftarrow \text{Out-Degree Rank}$
  - 15:    $\forall x \in \mathbb{U}, R(x) \leftarrow S_{\mathcal{L}}(\mathbb{L}, \Delta) \cdot (1 - M(x)) + (1 - S_{\mathcal{L}}(\mathbb{L}, \Delta)) \cdot \text{ODR}(x)$
  - 16:    $x_{\text{max}} \leftarrow \{\text{argmax}_{x \in \mathbb{U}} R(x)\}$
  - 17:    $Q \leftarrow Q \cup \{x_{\text{max}}\}$
  - 18:    $\forall x \in B_{\delta_{\text{avg}}}(x_{\text{max}}) : \forall e = (v, x) \in E$ , remove  $e$
  - 19:    $M(x_{\text{max}}) \leftarrow 1$
  - 20: **end for**
  - 21: **return**  $Q, P(C(\mathbb{L}, \Delta))$
-

- $M(x)$ ,  $\forall x \in \mathbb{U}$ : the normalized margin between the two highest softmax outputs using the last trained model if  $\mathbb{L} \neq \emptyset$ , 1 otherwise.
- $\Delta$ :  $\Delta = [\delta_i = \delta_0]_{i=1}^b$  if  $\mathbb{L} = \emptyset$ , otherwise use  $\Delta$  from the last AL iteration.
- $\delta_{\text{avg}}$ : the average of  $\Delta$ .
- $P(C(\mathbb{L}, \Delta))$ : the probability of coverage of the current  $\mathbb{L}$  with its corresponding  $\Delta$ .
- $S_{\mathcal{L}}(\mathbb{L}, \Delta)$ : the competence score of objective function (6) if  $\mathbb{L} \neq \emptyset$ , 0 otherwise.
- $\{G_{\delta_{\text{avg}}} = (V, E)\}$ : a directed adjacency graph where nodes represent samples and edges connect pairs of nodes if the distance between them in the embedding space is smaller than  $\delta_{\text{avg}}$ . In order not to cover points more than once,  $\forall x_i \in \mathbb{L}$ ,  $\forall x \in B_{\delta_i}(x_i)$  and  $\forall v \in V$  – prune incoming edges  $e = (v, x) \in E$ . Additionally, we prune all outgoing edges  $e = (x_i, v) \in E$ .

Next,  $q$  points are to be selected from  $\mathbb{U}$  in a greedy manner as follows:

1.  $\forall x \in \mathbb{U}$ , compute the Out-Degree-Rank  $\text{ODR}(x)$ .
2.  $\forall x \in \mathbb{U}$ , compute a ranking score  $R(x) = S_{\mathcal{L}}(\mathbb{L}, \Delta) \cdot (1 - M(x)) + (1 - S_{\mathcal{L}}(\mathbb{L}, \Delta)) \cdot \text{ODR}(x)$ .
3. Select the vertex  $x_{\text{max}}$  with the highest score,  $x_{\text{max}} = \arg\max_{x \in \mathbb{U}} R(x)$ .
4. Remove all incoming edges to  $x_{\text{max}}$  and its neighbors, implying that  $\text{ODR}(x_{\text{max}}) = 0$ .
5. Set  $M(x_{\text{max}}) = 1$ .

**(ii) Model training:**

1. Obtain labels for query set  $Q$ , returned in step (i) of **Active sampling**.
2. Remove set  $Q$  from  $\mathbb{U}$  and add it to  $\mathbb{L}$ .
3. Train the given model  $\mathbb{M}$  using  $\mathbb{L}$  (and  $\mathbb{U}$  if the learner is semi-supervised).

**(iii)  $\delta$ -expansion** for new samples. In this step (see Alg 2 below for pseudo-code), we compute a suitable  $\delta_i$  for each new labeled example  $x_i \in Q$ , and add it to  $\Delta$ . First, we use the updated model  $M$  to predict labels for all the points in the unlabeled set  $\mathbb{U}$ . We also compute a purity threshold  $\tau = m \cdot P(C(\mathbb{L} \setminus Q, \Delta)) + b$ , where  $m$  and  $b$  are hyperparameters and  $P(C(\mathbb{L} \setminus Q, \Delta))$  - the probability of coverage using the old labeled set - has been computed in the first **Active sampling** step. For each new labeled example  $v \in Q$ , we search for the largest radius  $\delta_{\text{opt}}$  such that its purity  $P(\{x \in B_{\delta_{\text{opt}}}(v) : f(x) = f(v)\})$  is still larger than  $\tau$ . Assuming that  $\pi(B_{\delta}(x))$  a monotonic with  $\delta$ , we can leverage binary search.

---

**Algorithm 2 DCoM,  $\delta$ -expansion**

---

- 1: **Input:** unlabeled pool  $\mathbb{U}$ , labeled pool  $\mathbb{L}$ , query pool  $Q$ , maximal ball size  $\delta_{\text{max}}$ , list of ball sizes  $\Delta$  for  $\mathbb{L} \setminus Q$ , trained model  $\mathbb{M}$  from the current iteration and  $P(C(\mathbb{L} \setminus Q, \Delta))$  from **Active sampling**
  - 2: **Output:** updated list of ball sizes  $\Delta$
  - 3:  $\tau \leftarrow m \cdot P(C(\mathbb{L} \setminus Q, \Delta)) + b$
  - 4:  $\hat{\mathbb{Y}} \leftarrow$  The predicted label for each  $x \in \mathbb{U}$  using the model  $\mathbb{M}$
  - 5: **for**  $v \in Q$  **do**
  - 6:    $\delta_{\text{opt}} \leftarrow \arg\max_{\delta} [P(\{x \in B_{\delta}(v) : f(x) = f(v)\}) > \tau]$
  - 7:    $\Delta \leftarrow \Delta + [\delta_{\text{opt}}]$
  - 8: **end for**
  - 9: **return**  $\Delta$
- 

Using a sparse representation of the adjacency graph enables *DCoM* to handle large datasets efficiently without exhaustive space requirements. The algorithm's complexity, including adjacency graph construction and sample selection, is discussed in App. C.

## 4 Empirical evaluation

### 4.1 Methodology

This section investigates two deep AL frameworks: a *fully supervised* approach, wherein a deep model is trained exclusively on the annotated dataset  $\mathbb{L}$  as a standard supervised task, and a *semi-supervised*



framework trained on both the annotated and unlabeled datasets,  $\mathbb{L}$  and  $\mathbb{U}$ . Our experimental setup is based on the codebase of [24], ensuring a fair comparison among the various AL strategies by using the same network architectures and sharing all relevant experimental conditions.

More specifically, in the following experiments, we trained ResNet-18 [16] on STL-10 [6], SVHN [25], CIFAR-100 [22] and subsets of ImageNet [9] including ImageNet-50, ImageNet-100, and ImageNet-200 as they appear in [33]. The hyper-parameters we used are detailed in App. A. In the semi-supervised framework, we used FlexMatch [42] and the code provided by [35]. For the experiments, we followed the parameters specified by [42]. The exact parameters are detailed in App. A. While the ResNet-18 architecture may no longer achieve state-of-the-art results on the datasets examined, it serves as a suitable platform to evaluate the efficacy of AL strategies in a competitive and fair environment, where they have demonstrated benefits.

In our comparisons, we used several active learning strategies (or optimization criteria) for selecting a query set: (1) *Random* sampling, (2) *Min margin* — lowest margin between the two highest softmax outputs, (3) *Max entropy* — highest entropy of softmax outputs [30], (4) *Uncertainty* — 1 minus maximum softmax output, (5) *DBAL* [11], (6) *CoreSet* [28], (7) *BALD* [21], (8) *BADGE* [1], (9) *ProbCover* [39], and (10) *LDM-s* [4]. When available, we used the code provided in [24] for each strategy. When it was unavailable, we used the code from the repositories of the corresponding papers. Since [4] doesn’t provide code, we compared our results with the corresponding available results reported in their paper, despite differences in the running setup (see App. D.6).

*DCoM* and *ProbCover* require a suitable data embedding. For STL-10, SVHN, CIFAR-10 and CIFAR-100 we employed the SimCLR [3] embedding. For the ImageNet subsets we used the DINOv2 [26] embedding. Section 4.3 provides an extensive ablation study, which includes alternative embedding spaces. In all experiments, identical settings and hyper-parameters are used for our method, as detailed in App. A. The robustness of our method to these choices is discussed in App. B.

## 4.2 Main results

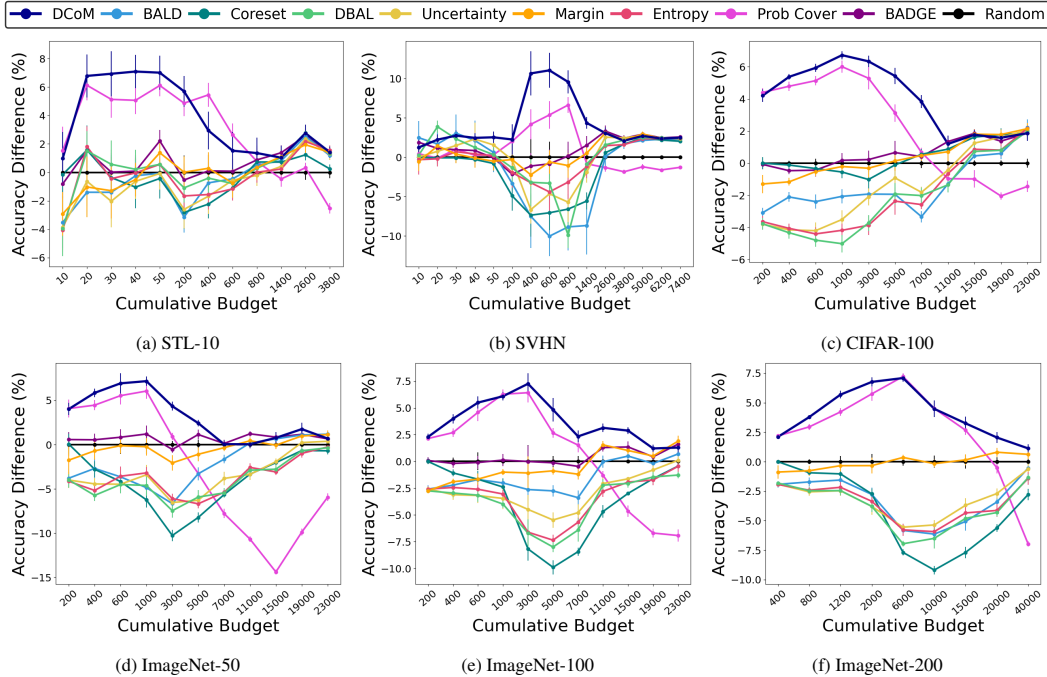


Figure 1: Mean accuracy difference between several AL algorithms and random queries. Positive mean difference indicates that the corresponding AL method is beneficial. The errors bars correspond to standard error, based on 5-10 repetitions (3 for the ImageNet subsets). While some methods perform well only in specific budget regimes, *DCoM* consistently achieves the best results across all budgets.

**Fully supervised framework.** We evaluate various AL methods by training a ResNet-18 model from scratch for each different AL strategy, using the labels of the queries selected by the respective method. In each AL iteration, a new model is trained from scratch using the updated labeled set  $\mathbb{L}$ .

This process is repeated for several AL iterations. Fig. 1 shows the difference between the accuracy obtained by each AL method, and the accuracy obtained when training a similar network with a random query set of the same size (the baseline of no active learning), for each AL iteration. The final accuracy of each method is shown in Tables 1-2 for the ImageNet-100 and CIFAR-100 datasets, as mean  $\pm$  Standard Error (STE). Additional datasets are shown in App. D.

Table 1: Model final accuracy when varying the size of the labeled set  $\mathbb{L}$  (row) and the respective AL strategy (column), using the ImageNet-100 dataset

$ \mathbb{L} $	Random	Prob Cover	BADGE	BALD	Coreset	Uncertainty	Entropy	DBAL	Margin	DCoM
200	4.58 $\pm$ 0.13	<b>6.72<math>\pm</math>0.07</b>	4.67 $\pm$ 0.16	1.99 $\pm$ 0.22	4.58 $\pm$ 0.13	2.01 $\pm$ 0.06	1.99 $\pm$ 0.10	1.83 $\pm$ 0.06	1.84 $\pm$ 0.12	<b>6.87<math>\pm</math>0.18</b>
400	6.61 $\pm$ 0.17	9.30 $\pm$ 0.23	6.42 $\pm$ 0.23	4.39 $\pm$ 0.39	5.53 $\pm$ 0.16	3.50 $\pm$ 0.32	4.17 $\pm$ 0.33	3.65 $\pm$ 0.25	4.71 $\pm$ 0.10	<b>10.59<math>\pm</math>0.26</b>
600	8.11 $\pm$ 0.42	12.71 $\pm$ 0.42	8.01 $\pm$ 0.20	6.42 $\pm$ 0.24	6.45 $\pm$ 0.37	4.93 $\pm$ 0.29	5.51 $\pm$ 0.33	4.96 $\pm$ 0.22	6.46 $\pm$ 0.12	<b>13.61<math>\pm</math>0.15</b>
1,000	11.43 $\pm$ 0.17	<b>17.71<math>\pm</math>0.27</b>	11.56 $\pm$ 0.38	9.42 $\pm$ 0.19	9.04 $\pm$ 0.66	7.97 $\pm$ 0.82	8.39 $\pm$ 0.18	7.45 $\pm$ 0.18	10.43 $\pm$ 0.11	<b>17.53<math>\pm</math>0.23</b>
3,000	27.59 $\pm$ 0.76	34.01 $\pm$ 0.15	27.58 $\pm$ 0.72	24.96 $\pm$ 0.23	19.41 $\pm$ 0.32	23.10 $\pm$ 0.60	20.97 $\pm$ 0.33	20.88 $\pm$ 0.52	26.51 $\pm$ 0.79	<b>34.85<math>\pm</math>0.23</b>
5,000	39.25 $\pm$ 0.26	41.91 $\pm$ 0.20	39.13 $\pm$ 0.06	36.50 $\pm$ 0.25	29.35 $\pm$ 0.39	33.78 $\pm$ 0.46	31.89 $\pm$ 0.24	31.25 $\pm$ 0.21	38.37 $\pm$ 0.10	<b>44.09<math>\pm</math>0.83</b>
7,000	46.88 $\pm$ 0.25	48.41 $\pm$ 0.42	46.42 $\pm$ 0.41	43.49 $\pm$ 0.42	38.45 $\pm$ 0.12	42.09 $\pm$ 0.54	41.19 $\pm$ 0.17	40.47 $\pm$ 0.83	45.69 $\pm$ 0.26	<b>49.22<math>\pm</math>0.29</b>
11,000	55.31 $\pm$ 0.26	54.01 $\pm$ 0.15	56.61 $\pm$ 0.11	55.29 $\pm$ 0.32	50.63 $\pm$ 0.33	53.25 $\pm$ 0.31	52.52 $\pm$ 0.26	53.09 $\pm$ 0.29	56.86 $\pm$ 0.10	<b>58.45<math>\pm</math>0.15</b>
15,000	61.69 $\pm$ 0.09	57.04 $\pm$ 0.43	63.05 $\pm$ 0.42	62.19 $\pm$ 0.21	58.71 $\pm$ 0.05	60.07 $\pm$ 0.07	59.76 $\pm$ 0.22	59.64 $\pm$ 0.30	62.71 $\pm$ 0.27	<b>64.57<math>\pm</math>0.22</b>
19,000	66.39 $\pm$ 0.26	59.69 $\pm$ 0.16	66.82 $\pm$ 0.33	66.19 $\pm$ 0.19	64.77 $\pm$ 0.32	65.59 $\pm$ 0.27	64.65 $\pm$ 0.23	64.93 $\pm$ 0.23	66.89 $\pm$ 0.28	<b>67.60<math>\pm</math>0.08</b>
23,000	68.92 $\pm$ 0.15	61.99 $\pm$ 0.41	<b>70.54<math>\pm</math>0.21</b>	69.62 $\pm$ 0.32	68.49 $\pm$ 0.06	69.03 $\pm$ 0.20	68.47 $\pm$ 0.50	67.65 $\pm$ 0.14	<b>70.81<math>\pm</math>0.35</b>	<b>70.21<math>\pm</math>0.32</b>

Table 2: Same as Table 1, using the CIFAR-100 dataset.

$ \mathbb{L} $	Random	Prob Cover	BADGE	BALD	Coreset	Uncertainty	Entropy	DBAL	Margin	LDM-s	DCoM
200	6.39 $\pm$ 0.19	<b>10.79<math>\pm</math>0.08</b>	6.31 $\pm$ 0.09	3.30 $\pm$ 0.11	6.39 $\pm$ 0.19	2.59 $\pm$ 0.05	2.74 $\pm$ 0.17	2.61 $\pm$ 0.18	5.09 $\pm$ 0.37	-	<b>10.59<math>\pm</math>0.19</b>
400	8.74 $\pm$ 0.07	13.53 $\pm$ 0.22	8.27 $\pm$ 0.14	6.63 $\pm$ 0.23	8.62 $\pm$ 0.17	4.59 $\pm$ 0.23	4.68 $\pm$ 0.23	4.41 $\pm$ 0.30	7.58 $\pm$ 0.17	-	<b>14.11<math>\pm</math>0.11</b>
600	10.73 $\pm$ 0.13	15.86 $\pm$ 0.16	10.29 $\pm$ 0.27	8.33 $\pm$ 0.31	10.39 $\pm$ 0.25	6.52 $\pm$ 0.38	6.32 $\pm$ 0.27	5.94 $\pm$ 0.28	10.20 $\pm$ 0.16	-	<b>16.66<math>\pm</math>0.11</b>
1,000	13.49 $\pm$ 0.18	19.49 $\pm$ 0.20	13.66 $\pm$ 0.26	11.42 $\pm$ 0.26	12.94 $\pm$ 0.21	9.98 $\pm$ 0.38	9.31 $\pm$ 0.22	8.47 $\pm$ 0.35	13.28 $\pm$ 0.19	-	<b>20.21<math>\pm</math>0.07</b>
3,000	24.02 $\pm$ 0.27	29.31 $\pm$ 0.42	24.24 $\pm$ 0.28	22.10 $\pm$ 0.11	23.00 $\pm$ 0.28	21.93 $\pm$ 0.26	20.15 $\pm$ 0.33	20.29 $\pm$ 0.23	23.71 $\pm$ 0.31	-	<b>30.36<math>\pm</math>0.08</b>
5,000	31.52 $\pm$ 0.39	34.64 $\pm$ 0.15	32.18 $\pm$ 0.33	29.58 $\pm$ 0.38	31.41 $\pm$ 0.26	30.60 $\pm$ 0.40	29.15 $\pm$ 0.46	29.60 $\pm$ 0.28	31.66 $\pm$ 0.23	-	<b>36.95<math>\pm</math>0.10</b>
7,000	37.69 $\pm$ 0.16	38.36 $\pm$ 0.13	38.09 $\pm$ 0.10	34.36 $\pm$ 0.20	38.24 $\pm$ 0.16	35.87 $\pm$ 0.19	35.11 $\pm$ 0.11	35.67 $\pm$ 0.35	38.16 $\pm$ 0.17	31.85 $\pm$ 0.00	<b>41.52<math>\pm</math>0.25</b>
11,000	45.66 $\pm$ 0.22	44.69 $\pm$ 0.20	<b>47.00<math>\pm</math>0.16</b>	44.37 $\pm$ 0.28	46.53 $\pm$ 0.18	45.23 $\pm$ 0.20	45.01 $\pm$ 0.17	44.31 $\pm$ 0.24	46.37 $\pm$ 0.36	40.88 $\pm$ 0.01	<b>46.86<math>\pm</math>0.28</b>
15,000	50.57 $\pm$ 0.09	49.58 $\pm$ 0.46	<b>52.42<math>\pm</math>0.17</b>	51.02 $\pm$ 0.09	<b>52.19<math>\pm</math>0.29</b>	51.82 $\pm$ 0.16	51.43 $\pm$ 0.21	51.30 $\pm$ 0.35	<b>52.37<math>\pm</math>0.19</b>	46.59 $\pm$ 0.01	<b>52.33<math>\pm</math>0.22</b>
19,000	54.95 $\pm$ 0.09	52.90 $\pm$ 0.14	56.32 $\pm$ 0.07	55.55 $\pm$ 0.27	<b>56.72<math>\pm</math>0.31</b>	<b>56.55<math>\pm</math>0.21</b>	55.76 $\pm$ 0.31	55.75 $\pm$ 0.14	<b>56.73<math>\pm</math>0.24</b>	49.41 $\pm$ 0.01	<b>56.53<math>\pm</math>0.07</b>
23,000	57.74 $\pm$ 0.14	56.29 $\pm$ 0.21	<b>59.60<math>\pm</math>0.16</b>	<b>59.96<math>\pm</math>0.35</b>	<b>59.59<math>\pm</math>0.22</b>	<b>59.79<math>\pm</math>0.23</b>	<b>59.91<math>\pm</math>0.08</b>	<b>59.72<math>\pm</math>0.21</b>	<b>59.88<math>\pm</math>0.21</b>	52.48 $\pm$ 0.00	<b>59.60<math>\pm</math>0.33</b>

**Semi-supervised framework.** We evaluate the effectiveness of 5 representative AL strategies with FlexMatch, a competitive semi-supervised learning method. We also evaluate our method, and the results of random sampling (no AL) as baseline. Fig. 2 shows the mean accuracy and STE based on 3 repetitions of FlexMatch, employing labeled sets generated by the different AL strategies. Note that in these experiments, since the query is selected from an unlabeled set, the resulting labeled set  $\mathbb{L}$  may be unbalanced between the classes, which is especially harmful when the budget is small. This affects all the methods. As a result, the accuracy with random sampling may differ from reported results. Notably, *DCoM* demonstrates significant superiority over random sampling.

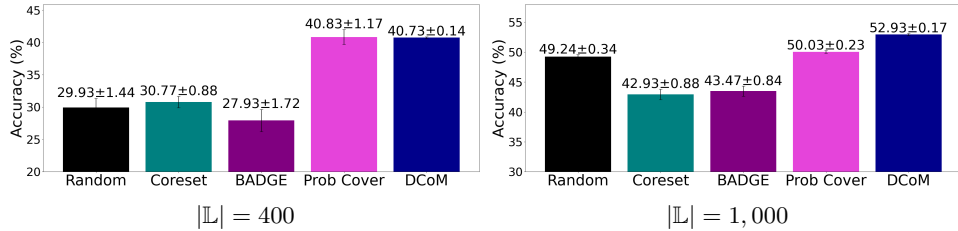


Figure 2: Comparison of AL strategies in a semi-supervised learning framework. Each bar represents the mean test accuracy over 3 repetitions of FlexMatch, trained using a total of 400 (left) and 1,000 (right) labeled examples on the CIFAR-100 dataset (an average of 4 and 10 labeled examples per class respectively). Three rounds of AL are considered, selecting 100 examples in the first round, 300 in the second, and 600 in the third.

### 4.3 Ablation study

We present a series of experiments where we investigate the choices made by our method, including different feature spaces and different uncertainty-based measures. The results demonstrate the robustness of our method to these choices. Additional choices are investigate in App. D, including the contribution of a dynamic  $\delta$  and initialization  $\delta_0$  (App. D.1). In App. D.3, we evaluate the effectiveness of  $S_{\mathcal{L}}(\mathbb{L}, \Delta)$  from (6) in capturing competence.

**Different feature spaces.** As discussed in Section 3.1, our approach relies on the existence of a suitable embedding space, where distance is indicative of semantic dissimilarity. We now repeat the



basic fully-supervised experiments while varying the embedding employed by *DCoM*, considering various popular self-supervised representations. Results are reported in Fig. 3, showing that *DCoM* consistently delivers the best performance regardless of the specific embedding used.

**Breaking down the algorithm into its components.** We evaluate the contribution of each component in objective function (1) separately. Results are shown in Fig. 4, wherein *DPC* denotes the Dynamic Probability Coverage, corresponding to  $\mathcal{O}_{low}(x)$  in *DCoM*, and *Margin* denotes *DCoM*’s choice for  $\mathcal{O}_{high}(x)$ . Clearly, the weighted objective function of *DCoM* yields superior results. Similar behavior is observed for several other datasets and other selections of  $\mathcal{O}_{high}(x)$ , see App. D.4.

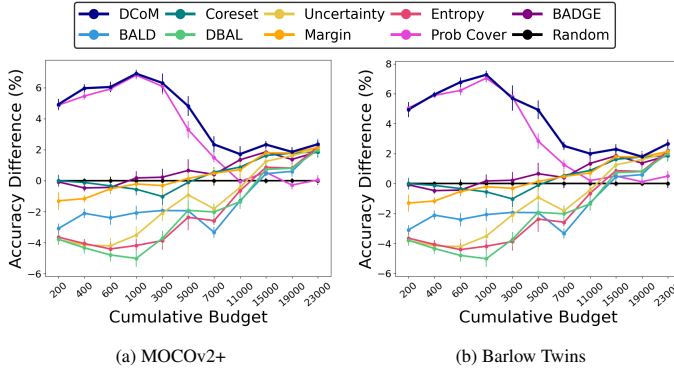


Figure 3: Performance over CIFAR-100, using two different embedding spaces for *DCoM* and *ProbCover*, see details in the caption of Fig. 1. Clearly, *DCoM* consistently achieves the best results. Results using another embedding space are provided in App. D.5.

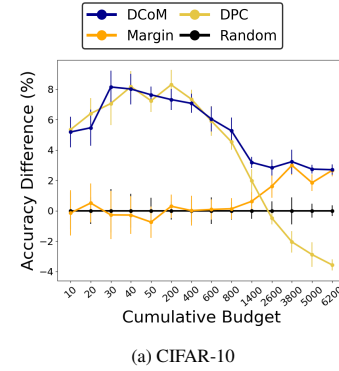


Figure 4: Performance evaluation (mean accuracy and STE) when optimizing each component of objective function (1) separately and together.

**Different uncertainty-based methods.** We now evaluate our choice for  $\mathcal{O}_{high}(x)$  in objective function (1), investigating the alternative methods of min margin, entropy of the min max activation, and uncertainty (see details in Section 4.1). Additionally, we use a score reminiscent of the AL method BADGE [11] and termed *Gradient norm*, which computes the norm of the gradient between the learner’s last two layers. Once again, the results of *DCoM* show robustness to this choice, with insignificant differences between the different uncertainty scores, see Fig. 6. Consequently, we prioritize computational efficiency and opt for the fastest-to-compute score, which is min-margin.

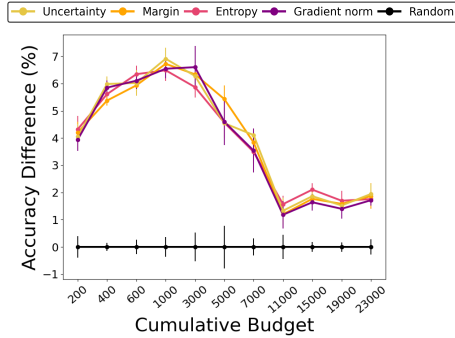


Figure 6: Similar to Fig. 1 and Tables 1-2, using only *DCoM* while leveraging 4 different variants for its underlying uncertainty score (see text). The performance differences between the variants are small.

Table 3: Model accuracy for different sizes of labeled set  $\mathbb{L}$  and several uncertainty-based methods for  $\mathbb{F}(x)$

$ \mathbb{L} $	Random	Entropy	Margin	Uncertainty	Gradient norm
200	6.39±0.19	<b>10.71±0.30</b>	<b>10.59±0.19</b>	<b>10.44±0.26</b>	<b>10.33±0.21</b>
400	8.74±0.07	<b>14.35±0.24</b>	14.11±0.11	<b>14.72±0.20</b>	<b>14.59±0.19</b>
600	10.73±0.13	<b>17.07±0.19</b>	16.66±0.11	<b>16.75±0.34</b>	<b>16.83±0.17</b>
1,000	13.49±0.18	<b>19.98±0.22</b>	<b>20.21±0.07</b>	<b>20.40±0.21</b>	<b>20.03±0.17</b>
3,000	24.02±0.27	29.89±0.11	<b>30.36±0.08</b>	<b>30.30±0.11</b>	<b>30.62±0.52</b>
5,000	31.52±0.39	36.08±0.13	<b>36.95±0.10</b>	36.06±0.18	36.12±0.46
7,000	37.69±0.16	41.18±0.25	<b>41.52±0.25</b>	<b>41.80±0.08</b>	<b>41.23±0.65</b>
11,000	45.66±0.22	<b>47.23±0.09</b>	<b>46.86±0.28</b>	<b>46.99±0.27</b>	46.84±0.28
15,000	50.57±0.09	<b>52.67±0.15</b>	<b>52.33±0.22</b>	<b>52.43±0.14</b>	52.21±0.22
19,000	54.95±0.09	<b>56.64±0.27</b>	<b>56.53±0.07</b>	<b>56.47±0.06</b>	<b>56.35±0.28</b>
23,000	57.74±0.14	<b>59.50±0.18</b>	<b>59.60±0.33</b>	<b>59.68±0.24</b>	<b>59.45±0.06</b>

## 5 Summary

We investigate the challenge of Active Learning (AL) in a multi-budget setting. Our approach is motivated by a new bound on the generalization error of the Nearest Neighbor classifier, and aims to minimize this bound. Additionally, the sampling strategy is dynamically adjusted during training using a new competence score, also motivated by the same bound. We validate our method empirically in both supervised and semi-supervised frameworks across various datasets. The results show that *DCoM* significantly outperforms alternative methods across all budgetary constraints.

## References

- [1] Jordan T Ash, Chicheng Zhang, Akshay Krishnamurthy, John Langford, and Alekh Agarwal. Deep batch active learning by diverse, uncertain gradient lower bounds. In *International Conference on Learning Representations*, 2019.
- [2] Liangyu Chen, Yutong Bai, Siyu Huang, Yongyi Lu, Bihan Wen, Alan Yuille, and Zongwei Zhou. Making your first choice: to address cold start problem in medical active learning. In *Medical Imaging with Deep Learning*, pages 496–525. PMLR, 2024.
- [3] Ting Chen, Simon Kornblith, Mohammad Norouzi, and Geoffrey Hinton. A simple framework for contrastive learning of visual representations. In *International conference on machine learning*, pages 1597–1607. PMLR, 2020.
- [4] Seong Jin Cho, Gwangsu Kim, Junghyun Lee, Jinwoo Shin, and Chang D Yoo. Querying easily flip-flopped samples for deep active learning. In *The Twelfth International Conference on Learning Representations*, 2023.
- [5] Shaif Chowdhury, Greg Hamerly, and Monica McGarrity. Active learning strategy using contrastive learning and k-means for aquatic invasive species recognition. In *Proceedings of the IEEE/CVF Winter Conference on Applications of Computer Vision (WACV) Workshops*, pages 848–858, January 2024.
- [6] Adam Coates, Andrew Ng, and Honglak Lee. An analysis of single-layer networks in unsupervised feature learning. In *Proceedings of the fourteenth international conference on artificial intelligence and statistics*, pages 215–223. JMLR Workshop and Conference Proceedings, 2011.
- [7] David A Cohn, Zoubin Ghahramani, and Michael I Jordan. Active learning with statistical models. *Journal of artificial intelligence research*, 4:129–145, 1996.
- [8] Victor Guilherme Turrise da Costa, Enrico Fini, Moin Nabi, Nicu Sebe, and Elisa Ricci. solo-learn: A library of self-supervised methods for visual representation learning. *Journal of Machine Learning Research*, 23(56):1–6, 2022. URL <http://jmlr.org/papers/v23/21-1155.html>.
- [9] Jia Deng, Wei Dong, Richard Socher, Li-Jia Li, Kai Li, and Li Fei-Fei. Imagenet: A large-scale hierarchical image database. In *2009 IEEE conference on computer vision and pattern recognition*, pages 248–255. Ieee, 2009.
- [10] Ibrahim M. El-Hasnony, Omar M. Elzeki, Ali Alshehri, and Hanaa Salem. Multi-label active learning-based machine learning model for heart disease prediction. *Sensors*, 22(3), 2022. ISSN 1424-8220. doi: 10.3390/s22031184. URL <https://www.mdpi.com/1424-8220/22/3/1184>.
- [11] Yarin Gal, Riashat Islam, and Zoubin Ghahramani. Deep bayesian active learning with image data. In *International Conference on Machine Learning*, pages 1183–1192. PMLR, 2017.
- [12] Daniel Gissin and Shai Shalev-Shwartz. Discriminative active learning. *arXiv preprint arXiv:1907.06347*, 2019.
- [13] Jean-Bastien Grill, Florian Strub, Florent Altché, Corentin Tallec, Pierre Richemond, Elena Buchatskaya, Carl Doersch, Bernardo Avila Pires, Zhaohan Guo, Mohammad Gheshlaghi Azar, et al. Bootstrap your own latent-a new approach to self-supervised learning. *Advances in neural information processing systems*, 33:21271–21284, 2020.
- [14] Guy Hacohen and Daphna Weinshall. How to select which active learning strategy is best suited for your specific problem and budget. *Advances in Neural Information Processing Systems*, 36, 2024.
- [15] Guy Hacohen, Avihu Dekel, and Daphna Weinshall. Active learning on a budget: Opposite strategies suit high and low budgets. In *International Conference on Machine Learning*. PMLR, 2022.

- [16] Kaiming He, Xiangyu Zhang, Shaoqing Ren, and Jian Sun. Deep residual learning for image recognition. In *2016 IEEE Conference on Computer Vision and Pattern Recognition, CVPR 2016, Las Vegas, NV, USA, June 27-30, 2016*, pages 770–778. IEEE Computer Society, 2016. doi: 10.1109/CVPR.2016.90. URL <https://doi.org/10.1109/CVPR.2016.90>.
- [17] Kaiming He, Haoqi Fan, Yuxin Wu, Saining Xie, and Ross Girshick. Momentum contrast for unsupervised visual representation learning. In *Proceedings of the IEEE/CVF conference on computer vision and pattern recognition*, pages 9729–9738, 2020.
- [18] Neil Houlsby, Ferenc Huszár, Zoubin Ghahramani, and Máté Lengyel. Bayesian active learning for classification and preference learning. *stat*, 1050:24, 2011.
- [19] Rong Hu, Brian Mac Namee, and Sarah Jane Delany. Off to a good start: Using clustering to select the initial training set in active learning. In *Twenty-Third International FLAIRS Conference*, 2010.
- [20] Abdelrahman Kaseb and Mona Farouk. Active learning for arabic sentiment analysis. *Alexandria Engineering Journal*, 77:177–187, 2023.
- [21] Andreas Kirsch, Joost Van Amersfoort, and Yarin Gal. Batchbald: Efficient and diverse batch acquisition for deep bayesian active learning. *Advances in neural information processing systems*, 32:7026–7037, 2019.
- [22] Alex Krizhevsky, Geoffrey Hinton, et al. Learning multiple layers of features from tiny images. *Online*, 2009.
- [23] David D Lewis and William A Gale. A sequential algorithm for training text classifiers. In *Proceedings of the 17th annual international ACM SIGIR conference on Research and development in information retrieval*, pages 3–12, 1994.
- [24] Prateek Munjal, Nasir Hayat, Munawar Hayat, Jamshid Sourati, and Shadab Khan. Towards robust and reproducible active learning using neural networks. In *2022 IEEE/CVF Conference on Computer Vision and Pattern Recognition (CVPR)*, pages 223–232. IEEE, 2022.
- [25] Yuval Netzer, Tao Wang, Adam Coates, Alessandro Bissacco, Baolin Wu, Andrew Y Ng, et al. Reading digits in natural images with unsupervised feature learning. In *NIPS workshop on deep learning and unsupervised feature learning*, volume 2011, page 7. Granada, Spain, 2011.
- [26] Maxime Oquab, Timothée Darcet, Théo Moutakanni, Huy V Vo, Marc Szafraniec, Vasil Khalidov, Pierre Fernandez, Daniel HAZIZA, Francisco Massa, Alaaeldin El-Nouby, et al. DINOv2: Learning robust visual features without supervision. *Transactions on Machine Learning Research*, 2023.
- [27] Hiranmayi Ranganathan, Hemanth Venkateswara, Shayok Chakraborty, and Sethuraman Panchanathan. Deep active learning for image classification. In *2017 IEEE International Conference on Image Processing (ICIP)*, pages 3934–3938, 2017. doi: 10.1109/ICIP.2017.8297020.
- [28] Ozan Sener and Silvio Savarese. Active learning for convolutional neural networks: A core-set approach. In *International Conference on Learning Representations*, 2018.
- [29] Burr Settles. Active learning literature survey. 2009.
- [30] Claude Elwood Shannon. A mathematical theory of communication. *The Bell System Technical Journal*, 27:379–423, 1948. URL <http://plan9.bell-labs.com/cm/ms/what/shannonday/shannon1948.pdf>.
- [31] Aditya Siddhant and Zachary C Lipton. Deep bayesian active learning for natural language processing: Results of a large-scale empirical study. In *Proceedings of the 2018 Conference on Empirical Methods in Natural Language Processing*, pages 2904–2909, 2018.
- [32] Alaa Tharwat and Wolfram Schenck. A survey on active learning: state-of-the-art, practical challenges and research directions. *Mathematics*, 11(4):820, 2023.

- [33] Wouter Van Gansbeke, Simon Vandenhende, Stamatios Georgoulis, Marc Proesmans, and Luc Van Gool. Scan: Learning to classify images without labels. In *European conference on computer vision*, pages 268–285. Springer, 2020.
- [34] Haoran Wang, Qiuye Jin, Shiman Li, Siyu Liu, Manning Wang, and Zhijian Song. A comprehensive survey on deep active learning and its applications in medical image analysis. *arXiv preprint arXiv:2310.14230*, 2023.
- [35] Yidong Wang, Hao Chen, Yue Fan, Wang Sun, Ran Tao, Wenxin Hou, Renjie Wang, Linyi Yang, Zhi Zhou, Lan-Zhe Guo, Heli Qi, Zhen Wu, Yu-Feng Li, Satoshi Nakamura, Wei Ye, Marios Savvides, Bhiksha Raj, Takahiro Shinozaki, Bernt Schiele, Jindong Wang, Xing Xie, and Yue Zhang. Usb: A unified semi-supervised learning benchmark for classification. In *Thirty-sixth Conference on Neural Information Processing Systems Datasets and Benchmarks Track*, 2022. doi: 10.48550/ARXIV.2208.07204. URL <https://arxiv.org/abs/2208.07204>.
- [36] Ziting Wen, Oscar Pizarro, and Stefan Williams. Ntkcpl: Active learning on top of self-supervised model by estimating true coverage. *arXiv e-prints*, pages arXiv–2306, 2023.
- [37] Jae Oh Woo. Active learning in bayesian neural networks with balanced entropy learning principle. In *The Eleventh International Conference on Learning Representations*, 2022.
- [38] Yi Yang, Zhigang Ma, Feiping Nie, Xiaojun Chang, and Alexander Hauptmann. Multi-class active learning by uncertainty sampling with diversity maximization. *International Journal of Computer Vision*, 113, 06 2015. doi: 10.1007/s11263-014-0781-x.
- [39] Ofer Yehuda, Avihu Dekel, Guy Hacohen, and Daphna Weinshall. Active learning through a covering lens. *Advances in Neural Information Processing Systems*, 35:22354–22367, 2022.
- [40] Di Yuan, Xiaojun Chang, Qiao Liu, Yi Yang, Dehua Wang, Minglei Shu, Zhenyu He, and Guangming Shi. Active learning for deep visual tracking. *IEEE Transactions on Neural Networks and Learning Systems*, 2023.
- [41] Jure Zbontar, Li Jing, Ishan Misra, Yann LeCun, and Stéphane Deny. Barlow twins: Self-supervised learning via redundancy reduction. In *International conference on machine learning*, pages 12310–12320. PMLR, 2021.
- [42] Bowen Zhang, Yidong Wang, Wenxin Hou, Hao Wu, Jindong Wang, Manabu Okumura, and Takahiro Shinozaki. Flexmatch: Boosting semi-supervised learning with curriculum pseudo labeling. *Advances in Neural Information Processing Systems*, 34:18408–18419, 2021.
- [43] Guang Zhao, Edward Dougherty, Byung-Jun Yoon, Francis Alexander, and Xiaoning Qian. Uncertainty-aware active learning for optimal bayesian classifier. In *International Conference on Learning Representations*, 2021. URL <https://openreview.net/forum?id=MuzZxFctAI>.

## Appendix

### A Implementation details

The source code used in this study is available at <https://github.com/avihu111/TypiClust>. The code is based on the GitHub repositories of Yehuda et al. [39] and Munjal et al. [24].

*DCoM* necessitates the computation of the initial delta for each dataset representation. The values utilized in our experiments can be found in Table 4. The  $\delta$  values of CIFAR-10 and CIFAR-100 are sourced from [39]. Information on the computation of  $\delta$  values for other datasets can be located in App. D.1.

Table 4: Initial delta values used in experiments

Dataset	SSL method	Initial $\delta$
STL-10	SimCLR	0.55
SVHN	SimCLR	0.4
CIFAR-10	SimCLR	0.75
CIFAR-100	SimCLR	0.65
ImageNet-50	DINOv2	0.75
ImageNet-100	DINOv2	0.7
ImageNet-200	DINOv2	0.65
CIFAR-100	MOCOv2+	0.5
CIFAR-100	BYOL	0.5
CIFAR-100	Barlow Twins	0.55

Additionally, throughout our experiments we used identical algorithm parameters, distinguishing between those for datasets with smaller class amounts (10) and larger ones (50+). These parameters encompass the adaptive purity threshold  $\tau$  from Alg 2 and the logistic function parameters for the competence score  $S_{\mathcal{L}}(\mathbb{L}, \Delta)$  in (6),  $(a, k)$ . Specifically, we employed  $\tau = 0.2$  cover + 0.4, with logistic parameters  $a = 0.9$  and  $k = 30$  for CIFAR-10, SVHN, and STL-10, and  $a = 0.8$  and  $k = 30$  for CIFAR-100 and ImageNet subsets. The  $\delta$  resolution for the binary search in *DCoM* was set to 0.05. Our ablation study, detailed in App. B, demonstrates that these selections have negligible impact on performance.

#### A.1 Supervised training

When training on STL-10, SVHN, CIFAR-10 and CIFAR-100 datasets, we utilized a ResNet-18 architecture trained for 200 epochs. Our optimization strategy involved using an SGD optimizer with a Nesterov momentum of 0.9, weight decay set to 0.0003, and cosine learning rate scheduling starting at a base rate of 0.025. Training was performed with a batch size of 100 examples, and we applied random cropping and horizontal flips for data augmentation. For an illustration of these parameters in use, refer to [24].

When training ImageNet-50, we used the same hyper-parameters, only changing the base learning rate to 0.01, the batch size to 50 and the epoch amount to 50.

When training ImageNet-100/200, we used the same hyper-parameters as ImageNet-50, only changing the epoch amount to 100.

The train and test partitions followed the original sets from the corresponding paper, with 10% of the train set used for validation in all datasets except for ImageNet-200, where 5% was used for validation.

#### A.2 Semi-supervised training

When training FlexMatch [42], we used the semi supervised framework by [35], and the AL framework by [24]. All experiments involved 3 repetitions.

We relied on the standard hyper-parameters used by FlexMatch [42]. Specifically, we trained WideResNet-28 for 512 epochs using the SGD optimizer, with 0.03 learning rate, 64 batch size, 0.9 SGD momentum, 0.999 EMA momentum, 0.001 weight decay and 2 widen factor.

### A.3 Self-supervised feature extraction

**STL-10, SVHN, CIFAR-10, CIFAR-100.** To extract semantically meaningful features, we trained SimCLR using the code provided by [33] for STL-10, SVHN, CIFAR-10 and CIFAR-100. Specifically, we used ResNet-18 [16] with an MLP projection layer to a 128-dim vector, trained for 512 epochs. All the training hyper-parameters were identical to those used by SCAN (all details can be found in [33]). After training, we used the 512 dimensional penultimate layer as the representation space.

**Representation learning: ImageNet-50/100/200.** We extracted features from the official (ViT-S/14) DINOv2 weights pre-trained on ImageNet [26]. We employed the L2-normalized penultimate layer for the embedding, which has a dimensionality of 384.

**Ablation embeddings – CIFAR-100.** We extracted more features as BYOL [13], MOCOv2+ [17], and Barlow Twins [41] using pre-trained weights from [8].

## B Hyper-parameters exploring

As described before, *DCoM* has 3 hyper-parameters:  $a$ ,  $k$  and  $\tau$ . When running the main experiments described in Section 4.2, we maintained consistency by employing identical parameters for STL-10, SVHN, and CIFAR-10, as well as for CIFAR-100 and the subsets of ImageNet. This approach helps to demonstrate that the choice of the hyper-parameters is not critical and does not significantly affect the results. Here, we conduct experiments with *DCoM* using STL-10 and CIFAR-100 datasets and several values for  $a$  and  $k$  from the definition of the competence score  $S_{\mathcal{L}}(\mathbb{L}, \Delta)$  in (6). We observe that while certain choices may be slightly better than others, all choices yield results that are very close to each other, and *DCoM* consistently outperforms or matches the performance of previous methods.

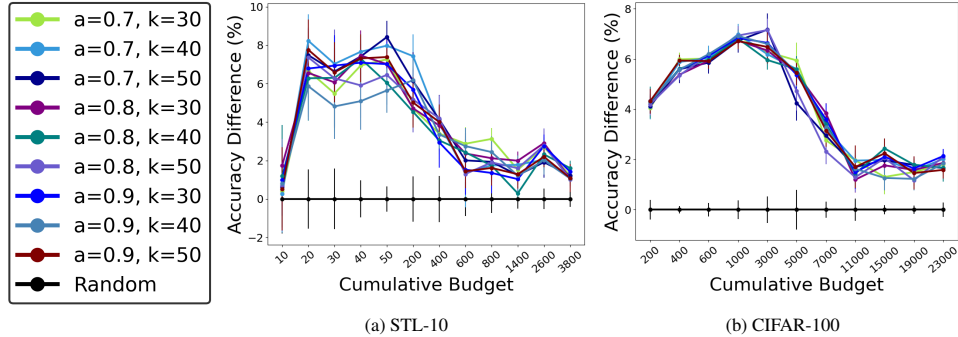


Figure 7: Evaluation of *DCoM* across different settings of the logistic function hyper-parameters  $a$  and  $k$ . Each plot displays the mean and standard error over 3 – 5 repetitions. The findings indicate that fine-tuning these parameters has negligible effects on performance.

## C Time and space complexity of *DCoM*

For the complexity analysis below, let  $n$  represent the number of examples in the combined unlabeled and labeled pool  $|\mathbb{L} \cup \mathbb{U}|$ ,  $d$  the dimension of the data embedding space,  $b$  - the given budget ( $|\mathbb{L}|$ ) and  $q$  - the size of the query set. As previously stated, *DCoM* can be divided into three distinct steps:

### C.1 Selection of initial $\delta$

**Time Complexity:** The process begins by creating  $t$  adjacency graphs, each corresponding to a different  $\delta$  value being evaluated. Here,  $t$  denotes the number of  $\delta$ 's being examined. The time



complexity of each graph generation is  $O(n^2 \cdot d)$  time. The computation of purity requires the prediction of pseudo-labels by k-means at a cost of  $O(n^2)$ . The complexity of computing ball purity for each example is  $O(n^2)$ , so totally each the ball purity computing takes  $O(n^3)$ . This adds up to overall time complexity of  $O(tdn^3)$ . Although it may seem significant, this step doesn't occur during the active learning algorithm process. Additionally, it's possible to confine the data employed for purity computation to the densest points, effectively lowering the complexity to  $O(tdn^2)$ . This approach mandates the use of at least the number of points equivalent to the number of classes for purity computation. This technique yields similar  $\delta_0$  values (consistent for CIFAR-10, CIFAR-100, and ImageNet-50, and with a variation of 0.05 for ImageNet-100/200 and STL-10 and 0.15 for SVHN).

**Space complexity:** Naively, the space complexity is  $O(n^2)$ , which might be impractical for large datasets like ImageNet. However, [39] demonstrates that utilizing a sparse matrix in coordinate list (COO) format and using limited  $\delta$  values, the space complexity becomes  $O(|E|)$ , where  $E$  represents the set of edges in the graph. Although  $O(|E|)$  remains  $O(n^2)$  in the worst-case scenario, in practice, the average vertex degree with a limited radius is less than  $n$ .

## C.2 Customizing $\delta$ values

**Time complexity:** Each iteration of *DCoM* starts with customizing  $\delta$  values for each labeled example from the last active step. In the worst case, there are  $|\mathbb{L}|$  examples. Customizing  $\delta$  involves building the adjacency graph using  $\delta_{\max}$ , running all examples on the model to obtain their predictions, and applying binary search over  $\delta$  values between 0 and  $\delta_{\max}$  for each example from the last active step. The binary search is performed on a continuous parameter ( $\delta$ ) with a search resolution  $r$ . This implies that there are  $\frac{\delta_{\max}}{r}$  available values for  $\delta$ . Overall, this process takes  $O(dn^2 + n + |\mathbb{L}| \cdot \log(\frac{\delta_{\max}}{r})) = O(dn^2 + b \cdot \log(\frac{\delta_{\max}}{r}))$ . In practical terms, due to the vectorization of these processes, it requires approximately 27 minutes to construct an adjacency graph for ImageNet-200 and update deltas for 1000 examples on a single CPU.

**Space complexity:** Similar to the space complexity analysis in App. C.1, which is  $O(n^2)$ .

## C.3 Active sampling

**Time complexity:** Active sampling involves balancing model min-margin and example density based on the current adjacency graph. Initially, the margin of each example is computed using the softmax output from the model's last layer, requiring  $O(n)$  time. Subsequently, the current adjacency is created using  $\delta_{\text{avg}}$ , which is the average over the  $\mathbb{L}$   $\delta$  values list -  $\Delta$ . As discussed in App. C.1, this step has a time complexity of  $O(dn^2)$ . Following this, the iterative process for selecting a single sample includes the following steps:

- Calculating node degrees –  $O(|E|)$  time.
- Finding the node with maximal degree –  $O(n)$  time.
- Removing incoming edges from the graph for covered points –  $O(|E|)$  time.

Samples are iteratively selected from the current sparse graph, with incoming edges to newly covered samples being removed. Unlike adjacency graph creation, sample selection cannot be parallelized, as each step depends on the previous one. Overall, the time complexity for selecting a sample is  $O(|E| + n)$ , resulting in a worst-case overall complexity of  $O(dn^2)$ . However, as more points are selected, the removal of edges speeds up the selection of later samples. Practically, it consumes about 15 minutes to construct an adjacency graph and select 1000 samples from ImageNet-200 on a single CPU.

**Space complexity:** Similar to the previous space complexity analysis –  $O(n^2)$ .

## D Additional empirical results

### D.1 $\delta_0$ Initialization

To set the initial value  $\delta_0$ , we adopted the method outlined in [39], as detailed in Section 3. Fig. 8 displays the purity function across various  $\delta$  values, along with the selected  $\delta$  values for each dataset. As mentioned previously, the  $\delta$  values for CIFAR-10 and CIFAR-100 are derived from [39].

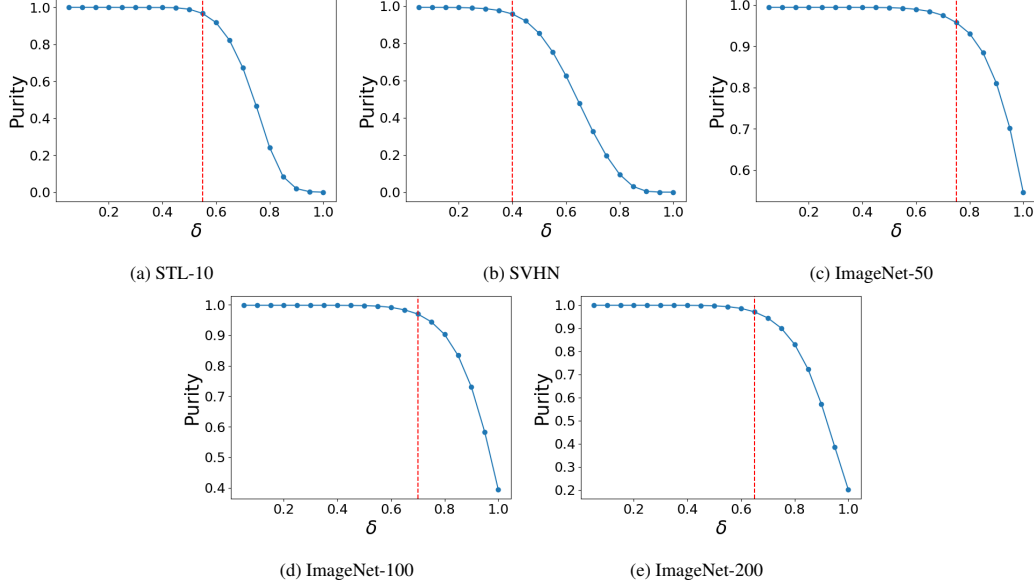


Figure 8:  $\pi(\delta)$ , estimated from the unlabeled data and using k-means algorithm for labeling. The dashed line indicates the highest  $\delta$ , after which purity drops below  $\alpha = 0.95$ .

### D.2 $\Delta$ distribution throughout the training process

The experiment in Fig. 9 illustrates the distribution of  $\Delta$  throughout the active selection and training phases of *DCoM*. The significant standard deviation of  $\Delta$  compared to the minor standard error underscores the significance of employing a dynamic method that assigns a distinct radius to each ball.

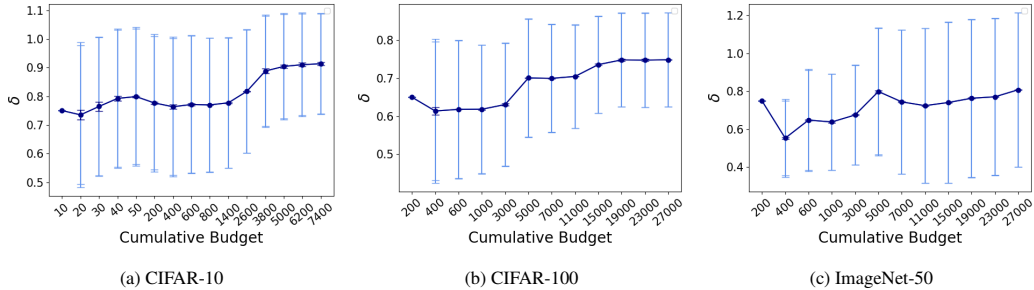


Figure 9: The  $\Delta$  distribution through *DCoM* algorithm. Each plot displays the mean and standard error over 5-10 repetitions. The results indicate that as the emphasis shifts towards maximizing the purity of sample balls, rather than solely focusing on maximum coverage, the radii adapt accordingly. This, combined with the improved performance observed with *DCoM*, highlights the necessity of the dynamic algorithm in enhancing the effectiveness of active sampling.

### D.3 Dynamic algorithm coverage

The analysis presented in Fig. 10 demonstrates a consistent behavior of probability coverage across different datasets during the *DCoM* process. This indicates that using probability coverage as a measure of progress consistently proves to be a wise decision.

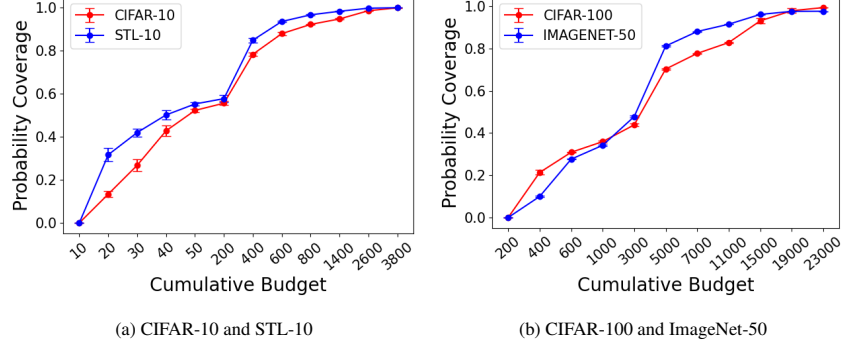


Figure 10: Comparison between  $P(C(\mathbb{L}, \Delta))$  values during *DCoM* sampling process, across several datasets. Each plot displays the mean and standard error over 3 – 10 repetitions. These figures demonstrates a consistent behavior of probability coverage.

### D.4 Decomposing the algorithm

In Section 4.3, we present an ablation study where we evaluate the contribution of each component in objective function (1) separately on CIFAR-100 dataset. In Fig. 11 you can see the results over CIFAR-100 and ImageNet-50 datasets.

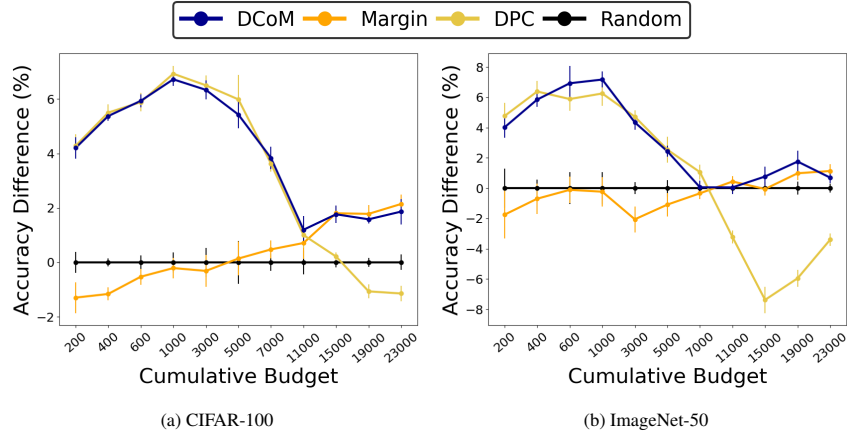


Figure 11: Performance evaluation (mean accuracy and STE) when optimizing each component of objective function (1) separately and together. DPC denotes the Dynamic Probability Coverage, corresponding to  $\mathcal{O}_{low}(x)$  in *DCoM*. Margin is *DCoM*'s choice for  $\mathcal{O}_{high}(x)$ .

In Fig. 12 you can see the same ablation but using entropy as  $\mathcal{O}_{high}(x)$  instead of margin.

### D.5 Different embedding space

In Section 4.3, we present an ablation study where we repeat the basic fully-supervised experiments while varying the embedding employed by *DCoM*. In Fig. 13 you can see the same ablation using BYOL [13] representation.

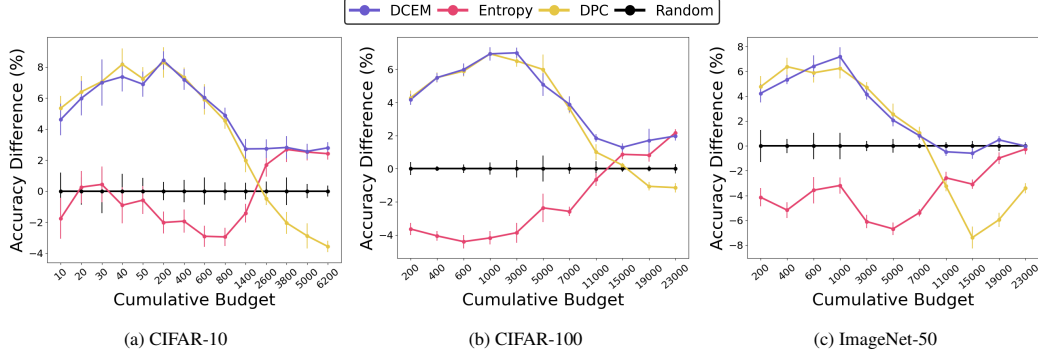


Figure 12: Assessment of each algorithm’s objective function individually across multiple datasets. DPC stands for Dynamic Probability Coverage, corresponding to  $\mathcal{O}_{low}(x)$  in *DCoM*. *DCEM* represents *DCoM* with entropy as  $\mathcal{O}_{high}(x)$  instead of margin. Each plot displays the mean and standard error over 5 – 10 repetitions. These graphs demonstrate how the weighted objective function consistently produces superior results across all labeled set sizes  $|\mathbb{L}|$ .

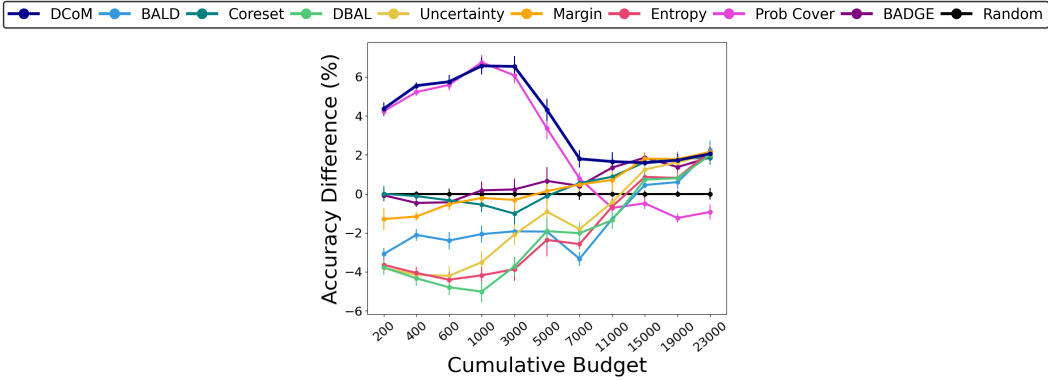


Figure 13: Performance over CIFAR-100, using BYOL feature space over *DCoM* and *ProbCover*, see details in the caption of Fig. 1. Clearly, *DCoM* consistently achieves the best results.

## D.6 Comparison per dataset

Tables 5-6 present the empirical accuracy values of several datasets using different active learning algorithms. In each active step, a new learner is trained from scratch over all available labeled data, and the results are presented as the [mean  $\pm$  STE] over 5 – 10 repetitions (3 for ImageNet subsets). As mentioned earlier, the results for LDM-s algorithm were acquired from the study by [4]. Their lack of code provision suggests discrepancies in the running setup. Nonetheless, the disparity between their method and random selection in their setup is smaller than that observed in ours, implying the superiority of our method. The table includes the results for all datasets, with the name of each dataset below it.

Table 5: Model accuracy for different sizes of labeled set  $\mathbb{L}$  and AL strategies

$ \mathbb{L} $	Random	Prob Cover	BADGE	BALD	Coreset	Uncertainty	Entropy	DBAL	Margin	LDM-s	DCoM
10	14.53±0.60	<b>20.39±0.23</b>	15.17±0.94	10.81±0.61	14.65±0.74	12.99±0.77	12.78±0.72	11.74±0.69	14.39±0.88	-	19.72±0.40
20	16.82±0.44	<b>24.64±0.73</b>	17.85±0.77	13.79±0.89	16.09±0.74	16.38±0.52	17.07±0.62	17.00±0.49	17.33±0.85	-	22.28±0.75
30	18.82±0.71	<b>27.19±0.25</b>	20.38±0.67	16.25±0.83	18.22±0.93	18.00±0.68	19.26±0.44	18.34±0.50	18.55±0.87	-	<b>26.98±0.35</b>
40	20.89±0.55	<b>29.46±0.38</b>	22.19±0.45	17.93±0.67	19.79±0.61	19.00±0.70	19.98±0.60	20.30±0.35	20.61±0.68	-	<b>28.91±0.46</b>
50	22.75±0.42	29.80±0.21	22.41±0.35	18.36±0.54	21.26±0.63	21.63±0.70	22.17±0.48	21.06±0.45	22.00±0.61	-	<b>30.39±0.12</b>
200	31.53±0.29	<b>38.83±0.18</b>	32.10±0.42	27.95±0.29	30.91±0.76	30.69±0.27	29.51±0.42	28.91±0.50	31.83±0.48	-	<b>38.86±0.40</b>
400	38.64±0.36	<b>45.36±0.51</b>	37.92±0.37	35.10±0.33	37.85±0.70	36.48±0.46	36.71±0.38	36.01±0.32	38.65±0.62	-	<b>45.72±0.27</b>
600	43.66±0.44	<b>49.13±0.36</b>	42.69±0.35	40.75±0.29	42.48±0.39	41.96±0.24	40.75±0.23	41.19±0.53	43.75±0.22	-	<b>49.71±0.39</b>
800	46.84±0.29	<b>51.49±0.37</b>	46.34±0.32	44.12±0.49	46.21±0.25	45.50±0.17	43.89±0.31	44.93±0.42	46.97±0.40	-	<b>52.10±0.58</b>
1,400	54.35±0.27	56.33±0.26	54.06±0.42	53.08±0.34	52.31±0.31	53.13±0.28	52.93±0.34	53.28±0.50	54.97±0.35	50.30±0.00	<b>57.54±0.10</b>
2,600	62.93±0.31	62.16±0.18	64.67±0.31	64.19±0.24	61.94±0.40	<b>64.98±0.59</b>	64.62±0.46	63.53±0.44	64.54±0.45	57.01±0.01	<b>65.76±0.21</b>
3,800	68.61±0.44	66.83±0.25	<b>71.36±0.32</b>	70.77±0.53	68.41±0.34	<b>71.90±0.36</b>	<b>71.30±0.36</b>	70.55±0.25	<b>71.60±0.21</b>	61.30±0.01	<b>71.84±0.36</b>
5,000	73.61±0.23	70.95±0.23	75.93±0.21	75.86±0.27	72.92±0.36	75.82±0.31	<b>76.13±0.31</b>	75.24±0.47	75.46±0.31	64.09±0.00	<b>76.36±0.05</b>
6,200	75.95±0.18	73.51±0.30	<b>78.90±0.27</b>	77.92±0.36	77.00±0.19	<b>78.84±0.27</b>	78.37±0.20	<b>78.54±0.26</b>	<b>78.62±0.22</b>	65.79±0.00	<b>78.66±0.16</b>
7,400	78.49±0.14	75.71±0.35	<b>80.88±0.22</b>	<b>80.94±0.16</b>	79.39±0.30	<b>81.19±0.15</b>	<b>81.02±0.19</b>	<b>81.10±0.24</b>	<b>80.76±0.29</b>	67.28±0.01	<b>81.30±0.34</b>

CIFAR-10 dataset

$ \mathbb{L} $	Random	Prob Cover	BADGE	BALD	Coreset	Uncertainty	Entropy	DBAL	Margin	LDM-s	DCoM
200	6.39±0.19	<b>10.79±0.08</b>	6.31±0.09	3.30±0.11	6.39±0.19	2.59±0.05	2.74±0.17	2.61±0.18	5.09±0.37	-	<b>10.59±0.19</b>
400	8.74±0.07	13.53±0.22	8.27±0.14	6.63±0.23	8.62±0.17	4.59±0.23	4.68±0.23	4.41±0.30	7.58±0.17	-	<b>14.11±0.11</b>
600	10.73±0.13	15.86±0.16	10.29±0.27	8.33±0.31	10.39±0.25	6.52±0.38	6.32±0.27	5.94±0.28	10.20±0.16	-	<b>16.66±0.11</b>
1,000	13.49±0.18	19.49±0.20	13.66±0.26	11.42±0.26	12.94±0.21	9.98±0.38	9.31±0.22	8.47±0.35	13.28±0.19	-	<b>20.21±0.07</b>
3,000	24.02±0.27	29.31±0.42	24.24±0.28	22.10±0.11	23.00±0.28	21.93±0.26	20.15±0.33	20.29±0.23	23.71±0.31	-	<b>30.36±0.08</b>
5,000	31.52±0.39	34.64±0.15	32.18±0.33	29.58±0.38	31.41±0.26	30.60±0.40	29.15±0.46	29.60±0.28	31.66±0.23	-	<b>36.95±0.10</b>
7,000	37.69±0.16	38.36±0.13	38.09±0.10	34.36±0.20	38.24±0.16	35.87±0.19	35.11±0.11	35.67±0.35	38.16±0.17	31.85±0.00	<b>41.52±0.25</b>
11,000	45.66±0.22	44.69±0.20	<b>47.00±0.16</b>	44.37±0.28	46.53±0.18	45.23±0.20	45.01±0.17	44.31±0.24	46.37±0.36	40.88±0.01	<b>46.86±0.28</b>
15,000	50.57±0.09	49.58±0.46	<b>52.42±0.17</b>	51.02±0.09	<b>52.19±0.29</b>	51.82±0.16	51.43±0.21	51.30±0.35	<b>52.37±0.19</b>	46.59±0.01	<b>52.33±0.22</b>
19,000	54.95±0.09	52.90±0.14	56.32±0.07	55.55±0.27	<b>56.72±0.31</b>	<b>56.55±0.21</b>	55.76±0.31	55.75±0.14	<b>56.73±0.24</b>	49.41±0.01	<b>56.53±0.07</b>
23,000	57.74±0.14	56.29±0.21	<b>59.60±0.16</b>	<b>59.96±0.35</b>	<b>59.59±0.22</b>	<b>59.79±0.23</b>	<b>59.91±0.08</b>	<b>59.72±0.21</b>	<b>59.88±0.21</b>	52.48±0.00	<b>59.60±0.33</b>

CIFAR-100 dataset

$ \mathbb{L} $	Random	Prob Cover	BADGE	BALD	Coreset	Uncertainty	Entropy	DBAL	Margin	DCoM
200	8.25±0.65	<b>12.33±0.34</b>	8.82±0.18	4.46±0.31	8.31±0.52	4.26±0.26	4.11±0.09	4.26±0.24	6.50±0.94	<b>12.27±0.04</b>
400	12.18±0.29	16.64±0.29	12.73±0.42	9.49±0.84	9.40±0.59	7.74±0.41	7.01±0.37	6.45±0.33	11.48±0.72	<b>18.03±0.21</b>
600	14.85±0.53	20.38±0.47	15.69±0.38	11.21±0.41	10.68±0.35	10.38±0.27	11.28±0.54	10.34±0.46	14.74±0.35	<b>21.77±0.62</b>
1,000	19.71±0.53	25.76±0.34	20.91±0.43	14.85±0.35	13.47±0.32	16.30±0.60	16.52±0.12	15.10±0.65	19.47±0.45	<b>26.88±0.00</b>
3,000	39.06±0.21	39.98±0.23	38.51±0.15	32.40±0.40	28.80±0.45	32.52±0.63	32.97±0.34	31.60±0.60	37.00±0.65	<b>43.40±0.29</b>
5,000	48.33±0.27	45.08±0.16	49.47±0.26	45.04±0.47	40.10±0.31	42.05±0.29	41.65±0.22	42.41±0.52	47.24±0.50	<b>50.76±0.08</b>
7,000	<b>55.12±0.09</b>	47.34±0.44	<b>55.25±0.34</b>	53.48±0.38	49.48±0.19	51.30±0.68	49.74±0.21	49.67±0.46	<b>54.78±0.29</b>	<b>55.17±0.34</b>
11,000	63.46±0.15	52.79±0.17	<b>64.68±0.15</b>	63.65±0.32	60.13±0.11	60.10±0.50	60.89±0.34	60.58±0.25	63.90±0.22	63.51±0.31
15,000	69.42±0.20	55.04±0.06	<b>70.27±0.25</b>	<b>70.08±0.21</b>	67.38±0.17	67.49±0.19	66.34±0.16	66.65±0.23	69.36±0.24	<b>70.19±0.45</b>
19,000	72.54±0.21	62.66±0.19	<b>73.70±0.21</b>	<b>73.63±0.21</b>	71.87±0.14	72.78±0.41	71.55±0.27	71.85±0.17	73.52±0.23	<b>74.29±0.50</b>
23,000	75.99±0.16	70.06±0.27	76.65±0.11	<b>77.17±0.06</b>	75.30±0.24	76.37±0.29	75.73±0.25	75.64±0.27	<b>77.12±0.30</b>	76.68±0.20

ImageNet-50 dataset

$ \mathbb{L} $	Random	Prob Cover	BADGE	BALD	Coreset	Uncertainty	Entropy	DBAL	Margin	DCoM
200	4.58±0.13	<b>6.72±0.07</b>	4.67±0.16	1.99±0.22	4.58±0.13	2.01±0.06	1.99±0.10	1.83±0.06	1.84±0.12	<b>6.87±0.18</b>
400	6.61±0.17	9.30±0.23	6.42±0.23	4.39±0.39	5.53±0.16	3.50±0.32	4.17±0.33	3.65±0.25	4.71±0.10	<b>10.59±0.26</b>
600	8.11±0.42	12.71±0.42	8.01±0.20	6.42±0.24	6.45±0.37	4.93±0.29	5.51±0.33	4.96±0.22	6.46±0.12	<b>13.61±0.15</b>
1,000	11.43±0.17	<b>17.71±0.27</b>	11.56±0.38	9.42±0.19	9.04±0.66	7.97±0.82	8.39±0.18	7.45±0.18	10.43±0.11	<b>17.53±0.23</b>
3,000	27.59±0.76	34.01±0.15	27.58±0.72	24.96±0.23	19.41±0.32	23.10±0.60	20.97±0.33	20.88±0.52	26.51±0.79	<b>34.85±0.23</b>
5,000	39.25±0.26	41.91±0.20	39.13±0.06	36.50±0.25	29.35±0.39	33.78±0.46	31.89±0.24	31.25±0.21	38.37±0.10	<b>44.09±0.83</b>
7,000	46.88±0.25	48.41±0.42	46.42±0.41	43.49±0.42	38.45±0.12	42.09±0.54	41.19±0.17	40.47±0.83	45.69±0.26	<b>49.22±0.29</b>
11,000	55.31±0.26	54.01±0.15	56.61±0.11	55.29±0.32	50.63±0.33	53.25±0.31	52.52±0.26	53.09±0.29	56.86±0.10	<b>58.45±0.15</b>
15,000	61.69±0.09	57.04±0.43	63.05±0.42	62.19±0.21	58.71±0.05	60.07±0.07	59.76±0.22	59.64±0.30	62.71±0.27	<b>64.57±0.22</b>
19,000	66.39±0.26	59.69±0.16	66.82±0.33	66.19±0.19	64.77±0.32	65.59±0.27	64.65±0.23	64.93±0.23	66.89±0.28	<b>67.60±0.08</b>
23,000	68.92±0.15	61.99±0.41	<b>70.54±0.21</b>	69.62±0.32	68.49±0.06	69.03±0.20	68.47±0.50	67.65±0.14	<b>70.81±0.35</b>	<b>70.21±0.32</b>

ImageNet-100 dataset

$ \mathbb{L} $	Random	Prob Cover	BALD	Coreset	Uncertainty	Entropy	DBAL	Margin	DCoM
400	3.10±0.07	<b>5.28±0.08</b>	1.18±0.21	3.10±0.07	1.19±0.07	1.17±0.13	1.29±0.06	2.22±0.50	<b>5.20±0.02</b>
800	4.61±0.10	7.56±0.15	2.90±0.29	3.68±0.12	2.06±0.24	2.20±0.19	2.15±0.20	3.85±0.34	<b>8.39±0.07</b>
1,200	5.88±0.25	10.10±0.08	4.32±0.33	4.84±0.14	3.42±0.19	3.71±0.26	3.42±0.16	5.54±0.23	<b>11.56±0.07</b>
2,000	9.51±0.33	15.25±0.26	6.73±0.26	6.78±0.15	5.72±0.41	6.15±0.04	5.72±0.15	9.17±0.34	<b>16.27±0.08</b>
6,000	25.67±0.16	<b>32.89±0.12</b>	19.85±0.26	17.98±0.10	20.12±0.11	19.89±0.35	18.72±0.08	26.03±0.08	<b>32.76±0.13</b>
10,000	37.49±0.26	<b>42.00±0.16</b>	31.36±0.46	28.31±0.10	32.13±0.16	31.57±0.28	31.00±0.59	37.33±0.08	<b>41.97±0.44</b>
15,000	46.22±0.30	48.89±0.09	41.16±0.49	38.53±0.18	42.53±0.29	41.88±0.31	41.42±0.13	46.37±0.17	<b>49.47±0.27</b>
20,000	52.20±0.19	51.70±0.32	48.79±0.58	46.59±0.15	49.50±0.25	48.07±0.36	47.89±0.13	53.01±0.19	<b>54.25±0.26</b>
40,000	64.57±0.17	57.60±0.05	64.02±0.37	61.78±0.30	63.94±0.27	63.14±0.37	63.21±0.13	65.19±0.24	<b>65.69±0.17</b>

ImageNet-200 dataset

Table 6: Model accuracy for different sizes of labeled set  $\mathbb{L}$  and AL strategies

$ \mathbb{L} $	Random	Prob Cover	BADGE	BALD	Coreset	Uncertainty	Entropy	DBAL	Margin	DCoM
10	<b>15.73±0.90</b>	<b>17.26±0.78</b>	14.92±0.98	12.22±0.91	<b>15.58±1.03</b>	11.88±0.83	11.67±0.48	11.79±1.06	12.81±0.65	<b>16.72±0.94</b>
20	16.68±0.77	<b>22.81±0.28</b>	18.24±0.46	15.28±0.98	18.25±0.97	16.05±0.94	18.48±0.67	18.19±0.63	15.65±1.35	<b>23.47±0.75</b>
30	19.78±0.79	24.91±0.49	19.80±0.38	18.37±1.06	19.41±0.92	17.75±1.05	19.33±0.74	20.35±0.90	18.49±1.16	<b>26.72±0.79</b>
40	21.49±0.48	26.56±0.48	21.57±0.48	21.25±0.95	20.45±1.00	20.86±0.77	21.45±0.74	21.70±0.88	20.97±0.71	<b>28.58±0.69</b>
50	22.19±0.33	<b>28.30±0.42</b>	24.40±0.45	22.13±0.56	21.76±1.07	22.11±0.81	22.75±0.60	22.76±0.91	23.57±0.59	<b>29.20±0.87</b>
200	36.04±0.59	40.91±0.33	35.50±0.57	32.89±0.50	33.22±0.55	33.44±0.76	34.38±0.58	34.95±0.46	36.05±0.53	<b>41.74±0.49</b>
400	44.07±0.60	<b>49.52±0.23</b>	44.18±0.54	43.33±0.45	41.83±0.39	42.39±0.64	42.51±0.46	43.67±0.47	44.35±0.52	47.02±0.73
600	50.02±0.44	<b>52.65±0.35</b>	50.10±0.44	49.56±0.32	48.91±0.32	49.46±0.48	48.85±0.38	49.23±0.49	49.27±0.59	<b>51.54±0.86</b>
800	53.69±0.36	<b>54.45±0.56</b>	<b>54.57±0.63</b>	<b>54.20±0.51</b>	<b>54.42±0.21</b>	53.48±0.38	53.70±0.38	53.98±0.31	<b>54.05±0.56</b>	<b>55.05±0.71</b>
1,400	62.00±0.26	61.54±0.30	<b>63.38±0.25</b>	<b>62.82±0.51</b>	<b>62.72±0.42</b>	62.42±0.27	62.24±0.23	<b>63.04±0.23</b>	<b>63.11±0.25</b>	<b>63.04±0.57</b>
2,600	70.18±0.27	70.50±0.08	<b>72.76±0.19</b>	<b>72.72±0.26</b>	71.41±0.13	72.53±0.23	72.35±0.18	<b>72.97±0.18</b>	72.12±0.40	<b>72.93±0.33</b>
3,800	75.51±0.21	72.97±0.17	<b>76.75±0.15</b>	76.69±0.11	75.75±0.09	<b>76.80±0.21</b>	<b>77.05±0.15</b>	<b>76.85±0.09</b>	<b>76.91±0.10</b>	<b>76.92±0.18</b>

STL-10 dataset

$ \mathbb{L} $	Random	Prob Cover	BADGE	BALD	Coreset	Uncertainty	Entropy	DBAL	Margin	LDM-s	DCoM
10	11.36±0.50	11.80±0.08	<b>13.26±0.79</b>	<b>13.84±1.64</b>	11.36±0.50	<b>11.41±0.85</b>	<b>11.06±1.38</b>	<b>11.66±0.56</b>	10.80±0.66	-	<b>12.62±0.60</b>
20	11.05±0.41	10.96±0.19	12.19±0.67	12.74±1.26	10.99±0.59	11.81±0.84	10.86±0.58	<b>14.94±0.36</b>	12.50±0.95	-	13.30±0.26
30	11.16±0.36	<b>12.19±0.52</b>	<b>12.12±0.51</b>	<b>14.22±2.01</b>	11.10±0.29	<b>12.66±1.28</b>	<b>11.86±0.65</b>	<b>13.50±0.46</b>	<b>11.56±0.79</b>	-	<b>13.91±0.32</b>
40	11.85±0.46	12.11±0.20	12.71±0.70	<b>13.98±2.06</b>	11.57±0.57	<b>14.16±1.63</b>	12.28±0.47	13.10±0.41	11.76±0.75	-	<b>14.32±0.14</b>
50	12.55±0.49	12.86±0.36	12.47±0.89	<b>13.18±2.00</b>	11.76±0.38	<b>14.12±1.00</b>	12.72±0.54	12.88±0.54	12.04±0.68	-	<b>15.09±0.25</b>
200	22.32±0.84	<b>24.34±0.44</b>	20.18±1.09	19.00±1.66	17.42±1.03	21.99±1.11	20.38±1.08	20.98±0.99	22.03±0.87	-	<b>24.58±1.10</b>
400	36.24±1.24	40.42±0.67	35.13±0.40	28.74±2.78	28.88±1.47	29.58±0.55	33.01±1.36	33.06±1.82	34.01±0.18	-	<b>46.90±1.56</b>
600	47.29±0.98	52.67±0.75	46.46±0.87	37.26±1.56	40.24±1.24	42.65±0.68	42.89±1.38	43.99±0.46	46.69±0.50	-	<b>58.34±1.25</b>
800	56.32±0.50	62.96±0.51	56.48±1.33	47.47±2.46	49.74±1.42	50.62±2.03	53.17±1.64	46.45±1.14	55.27±1.05	-	<b>65.90±0.97</b>
1,400	74.00±0.38	73.16±0.21	75.53±0.77	65.33±3.30	68.44±0.69	72.13±0.98	72.81±1.09	73.14±0.69	74.53±0.74	<b>79.02±0.01</b>	78.36±0.36
2,600	83.24±0.48	81.94±0.08	<b>86.56±0.24</b>	83.33±0.96	83.83±0.39	85.80±0.31	84.72±0.54	84.83±0.59	<b>86.33±0.13</b>	83.76±0.00	<b>86.31±0.26</b>
3,800	87.18±0.14	85.34±0.11	<b>89.61±0.25</b>	88.91±0.54	88.86±0.14	<b>89.64±0.09</b>	88.79±0.14	89.36±0.15	89.34±0.18	86.08±0.00	89.28±0.13
5,000	88.79±0.15	87.58±0.20	<b>91.72±0.15</b>	90.93±0.14	91.24±0.17	<b>91.55±0.04</b>	91.13±0.11	91.28±0.12	<b>91.75±0.17</b>	87.58±0.00	<b>91.50±0.08</b>
6,200	90.16±0.04	88.55±0.10	<b>92.64±0.09</b>	92.46±0.04	92.35±0.03	<b>92.63±0.08</b>	<b>92.56±0.16</b>	<b>92.65±0.10</b>	<b>92.55±0.12</b>	88.64±0.00	<b>92.54±0.12</b>
7,400	90.99±0.11	89.71±0.08	<b>93.56±0.05</b>	93.26±0.10	93.02±0.14	93.33±0.05	93.38±0.07	93.38±0.11	<b>93.43±0.13</b>	89.56±0.00	<b>93.47±0.09</b>

SVHN dataset